

BIOCHEMISTRY

Aurora A regulation by reversible cysteine oxidation reveals evolutionarily conserved redox control of Ser/Thr protein kinase activity

Dominic P. Byrne^{1*}, Safal Shrestha^{2,3}, Martin Galler⁴, Min Cao⁴, Leonard A. Daly^{1,5}, Amy E. Campbell^{1,5}, Claire E. Eyers^{1,5}, Elizabeth A. Veal⁴, Natarajan Kannan^{2,3}, Patrick A. Eyers^{1*}

Copyright © 2020
The Authors, some
rights reserved;
exclusive licensee
American Association
for the Advancement
of Science. No claim
to original U.S.
Government Works

Reactive oxygen species (ROS) are physiological mediators of cellular signaling and play potentially damaging roles in human diseases. In this study, we found that the catalytic activity of the Ser/Thr kinase Aurora A was inhibited by the oxidation of a conserved cysteine residue (Cys²⁹⁰) that lies adjacent to Thr²⁸⁸, a critical phosphorylation site in the activation segment. Cys is present at the equivalent position in ~100 human Ser/Thr kinases, a residue that we found was important not only for the activity of human Aurora A but also for that of fission yeast MAPK-activated kinase (Srk1) and PKA (Pka1). Moreover, the presence of this conserved Cys predicted biochemical redox sensitivity among a cohort of human CAMK, AGC, and AGC-like kinases. Thus, we predict that redox modulation of the conserved Cys²⁹⁰ of Aurora A may be an underappreciated regulatory mechanism that is widespread in eukaryotic Ser/Thr kinases. Given the key biological roles of these enzymes, these findings have implications for understanding physiological and pathological responses to ROS and highlight the importance of protein kinase regulation through multivalent modification of the activation segment.

INTRODUCTION

Reactive oxygen species (ROS), the collective term for reactive oxygen-derived radicals, including superoxide and peroxide, were originally regarded as side products of oxygen metabolism but are now recognized as key players in eukaryotic signal transduction (1, 2). Endogenous redox signaling in cells is induced in response to growth factors, such as epidermal growth factor (EGF) (1, 3), and ROS are important regulators of cell migration, differentiation, and the proliferative cell cycle (4–6). The sulfur atom of Cys residues, the predominant intracellular redox-signaling molecule, can exist in a variety of oxidation states (fig. S1). In ROS-targeted signaling proteins, oxidation of a reactive Cys thiolate anion (Cys-S⁻) results in the formation of the transient sulfenic acid species (Cys-SOH), which can either undergo further (irreversible) oxidation to sulfinic (Cys-SO₂H) or sulfonic (Cys-SO₃H) acid. The sulfenic species can be stabilized by formation of a disulfide with another Cys or through formation of a cyclic sulfenamide, as established in the case of the tyrosine phosphatase PTP1B, which can be recycled to the thiolate in vivo by glutaredoxin (GRX) or thioredoxin (7–11). The reduced glutathione (GSH) pool serves to buffer the cellular environment, with physiological concentrations ranging from ~1 to 10 mM (12–16). In the cytosol, glutathione exists as both oxidized (GSSG) and reduced (GSH) species, and the GSSG/GSH ratio changes as a function of redox stress (15). Reversible modification of protein cysteine thiol groups through disulfide bond formation with GSH is therefore considered

to be a defense mechanism, protecting proteins against proteotoxic stress caused by irreversible oxidation (17).

Protein phosphorylation on Ser/Thr and Tyr residues controls multiple aspects of eukaryotic life (18). To regulate the precise flow of signaling information, the enzymes that catalyze the addition and removal of phosphate groups are themselves subject to reversible regulation. In the case of Ser, Thr, and Tyr kinases, this often involves phosphorylation-based mechanisms in which conserved residues are cyclically phosphorylated and dephosphorylated to control catalysis. A well-known example is the reversible phosphorylation of Ser/Thr and Tyr residues in the conformationally flexible “activation segment,” which can either be liberated or folded back onto the kinase to inhibit substrate binding and phosphorylation (19). The activation segment, also known as the T-loop, is located between the DFG and APE motifs (20), two highly characteristic regions found in canonical eukaryotic protein kinases (ePKs) (21). In the case of phosphotyrosine (pTyr) regulation, redox control of Tyr phosphatases is well documented (9, 10, 22), providing an extra layer of regulation in addition to reversible phosphorylation of membrane-transducing Tyr kinases such as EGF receptor (EGFR) (23).

For ePKs, several examples of redox-associated mechanisms have been reported, although the lack of a catalytic Cys in the active site means that these mechanisms have been centered on other regulatory regions of the kinase domain, most notably modification of conserved Cys residues in the Gly-rich P-loop. Well-characterized examples of redox-sensitive Tyr kinases regulated by this mechanism include ABL, SRC, EGFR, and fibroblast growth factor receptor (24–27). In addition, several examples of Ser/Thr kinase regulation through redox-active Cys residues exist, although no overarching evolutionary-based mechanism has been proposed. Examples of eukaryotic redox-regulated proteins containing Ser/Thr kinase domains include apoptosis signal-regulating kinase 1 (ASK1), MEKK1, maternal embryonic leucine zipper kinase (MELK), protein kinase A (PKA), protein kinase G (PKG), extracellular signal-regulated kinase, c-Jun N-terminal kinase (JNK), and p38 mitogen-activated protein kinase (MAPK) family members (28–41).

¹Department of Biochemistry and Systems Biology, Institute of Systems, Molecular and Integrative Biology, University of Liverpool, Liverpool L69 7ZB, UK. ²Institute of Bioinformatics, University of Georgia, Athens, GA 30602, USA. ³Department of Biochemistry and Molecular Biology, University of Georgia, Athens, GA 30602, USA. ⁴Biosciences Institute, Newcastle University, Newcastle upon Tyne NE2 4HH, UK. ⁵Centre for Proteome Research, Department of Biochemistry and Systems Biology, Institute of Systems, Molecular and Integrative Biology, University of Liverpool, Liverpool L69 7ZB, UK.

*Corresponding author. Email: dominic.byrne@liverpool.ac.uk (D.P.B.); patrick.eyers@liverpool.ac.uk (P.A.E.)

The discovery of chemically accessible (and redox-sensitive) Cys residues in protein kinases has created new opportunities for the design of chemical reagents and covalent clinical compounds to target these residues with impressive specificity (42–46). However, without a common set of biochemical reagents and reliable real-time assay conditions for comparison, it is currently challenging to define a common theme or mechanism for redox-based regulation among protein kinases, which are assayed under a variety of biochemical conditions.

Aurora A is an oncogenic Ser/Thr protein kinase (47), which is subject to multilevel, reversible regulation in human cells including phosphorylation/dephosphorylation in the activation segment and allosteric control by accessory factors such as targeting protein for Xk1p2 (TPX2), transforming acidic coiled coil–containing protein 3 (TACC3), and protein phosphatases (48–51). Aurora A activation controls the G₂-M transition (52) and is also required for centrosome separation and mitotic spindle assembly (53, 54). Furthermore, Aurora A–dependent signaling is also implicated in mitochondrial dynamics and metabolism, which are closely associated with the production of ROS (55).

In this study, we investigated the role of activation segment Cys residues in a variety of ePKs. We report that catalytic activity of Aurora A is acutely controlled by a specific and reversible oxidative modification of Cys²⁹⁰, which lies adjacent to Thr²⁸⁸, the well-established activating “T-loop” site of phosphorylation. This Cys residue has been conserved in all Aurora kinases throughout eukaryotic evolution, and we propose that redox modulation of the Cys²⁹⁰ equivalent in distinct eukaryotic Ser/Thr kinases might be a dominant, evolutionary-conserved, regulatory mechanism for a substantial proportion of the human kinome. These findings have implications for understanding physiological and pathological responses to ROS in cells and help rationalize numerous lines of experimental evidence, demonstrating that reducing agents are often required for the catalytic activity of Ser/Thr kinases when assayed *in vitro*.

RESULTS

Redox regulation of Aurora A

Human Aurora A was purified to homogeneity in the presence or absence of the reductant dithiothreitol (DTT); immunoblotting with a phospho-specific antibody confirmed similar levels of pThr²⁸⁸ in enzyme preparations, as expected for active, autophosphorylated, Aurora A (fig. S2A). Regardless of whether it was purified under our standard reducing conditions (+DTT) or not, Aurora A activity was inhibited by H₂O₂ in a concentration-dependent manner, with ~70% inhibition observed at 100 μM H₂O₂, even when the ratio of enzyme:peroxide was increased 1000-fold (Fig. 1A and fig. S2, B and C). Diamide, which also oxidizes exposed cysteine residues in proteins (56, 57), also rapidly inhibited Aurora A activity in a dose-dependent manner (Fig. 1A and fig. S2C).

A similar degree of inhibition was observed when higher concentrations of Aurora A were exposed to a gradient of peroxide for 16 hours, to mimic chronic physiological exposure to oxidation (fig. S2B). In contrast, exposure of Aurora A to increasing concentrations of DTT progressively enhanced catalytic activity, regardless of the purification protocol used (compare Fig. 1A and fig. S2C). To further evaluate the redox response of Aurora A toward a substrate, we used the physiological Aurora A target TACC3 and confirmed that phosphorylation at Ser⁵⁵⁸ was inhibited in a dose-dependent

manner by H₂O₂, similar to the Aurora A inhibitor MLN8237 (Fig. 1B). In marked contrast, DTT increased phosphotransferase activity toward TACC3 (Fig. 1B). A prerequisite for Aurora A activation is autophosphorylation on Thr²⁸⁸ in the activation loop (58, 59), which is generated in this experiment during bacterial maturation before purification. Thr²⁸⁸ was highly phosphorylated under all of the tested conditions, regardless of the presence of DTT and/or H₂O₂, suggesting that oxidative inhibition of Aurora A was not a result of peroxide-induced dephosphorylation at this regulatory site (Fig. 1B). Next, we sought to establish whether H₂O₂ exposure led to irreversible inhibition of Aurora A activity. We quantified the real-time phosphorylation of a substrate peptide by Aurora A that had been previously exposed to H₂O₂. When H₂O₂ was included in the reaction, only ~15% of the peptide substrate was phosphorylated after 25 min, compared to ~60% in its absence (Fig. 1C, left). However, supplementing the reaction with DTT restored peroxide-inhibited Aurora A activity, resulting in an immediate increase in the rate of substrate phosphorylation comparable to a control maintained in an oxidized (inhibited) state (Fig. 1C, left). Similarly, the activity of Aurora A purified in the presence of DTT and then inhibited by H₂O₂ was rescued in real time by the addition of DTT (fig. S2D). In contrast, DTT was ineffective at reactivating Aurora A that was inhibited by the compound MLN8237 (Fig. 1C, right). These findings indicate that the catalytic activity of Aurora A is reversibly inhibited by oxidation. The inclusion of H₂O₂ did not affect the amount of Aurora phosphorylated on Thr²⁸⁸, although we noted that H₂O₂ treatment did cause a slight increase in the electrophoretic mobility of Aurora A (Fig. 1D, asterisks). This mobility shift was abolished by DTT, consistent with the presence of a reversibly oxidized Cys residue (or residues) (60, 61) in Aurora A.

To rule out “nonspecific” kinase inactivation as a result of oxidative protein unfolding or multisite oxidation, we performed thermal stability measurements for Aurora A incubated with H₂O₂. The unfolding profile obtained for Aurora A was unaltered by inclusion of H₂O₂, DTT or GSH, with *T_m* (melting temperature) values of ~40°C observed under test conditions (fig. S3A). To evaluate the consequences of Aurora A oxidation on the ability to bind Mg–adenosine triphosphate (ATP), we calculated the rate of phosphate incorporation into the peptide substrate in the presence of different H₂O₂ concentrations. Michaelis-Menten kinetic analysis revealed that H₂O₂ treatment significantly reduced the catalytic constant, *K_{cat}*, of Aurora A, without affecting the affinity for ATP at the highest concentrations tested (inferred from *K_{M[ATP]}* values) (fig. S3B). Consistent with a lack of direct effects on the nucleotide-binding site, differential scanning fluorimetry (DSF) analysis demonstrated that almost identical ΔT_m values were calculated after binding of ATP or the inhibitor MLN8237 in the presence of H₂O₂, DTT, or GSH (fig. S3C). Together, these data indicate that oxidation inhibits the ability of Aurora A to drive substrate (both peptide and protein) phosphorylation without affecting the affinity for ATP or the thermal stability (unfolding) profile of the kinase.

Aurora A autoactivation is stimulated by DTT and inhibited by H₂O₂

As an additional measure of the ability of H₂O₂ to inhibit Aurora A activity, we investigated the rate of autophosphorylation in dephosphorylated Aurora A that was generated by bacterial coexpression with lambda phosphatase (λPP), which removes all activating phosphate

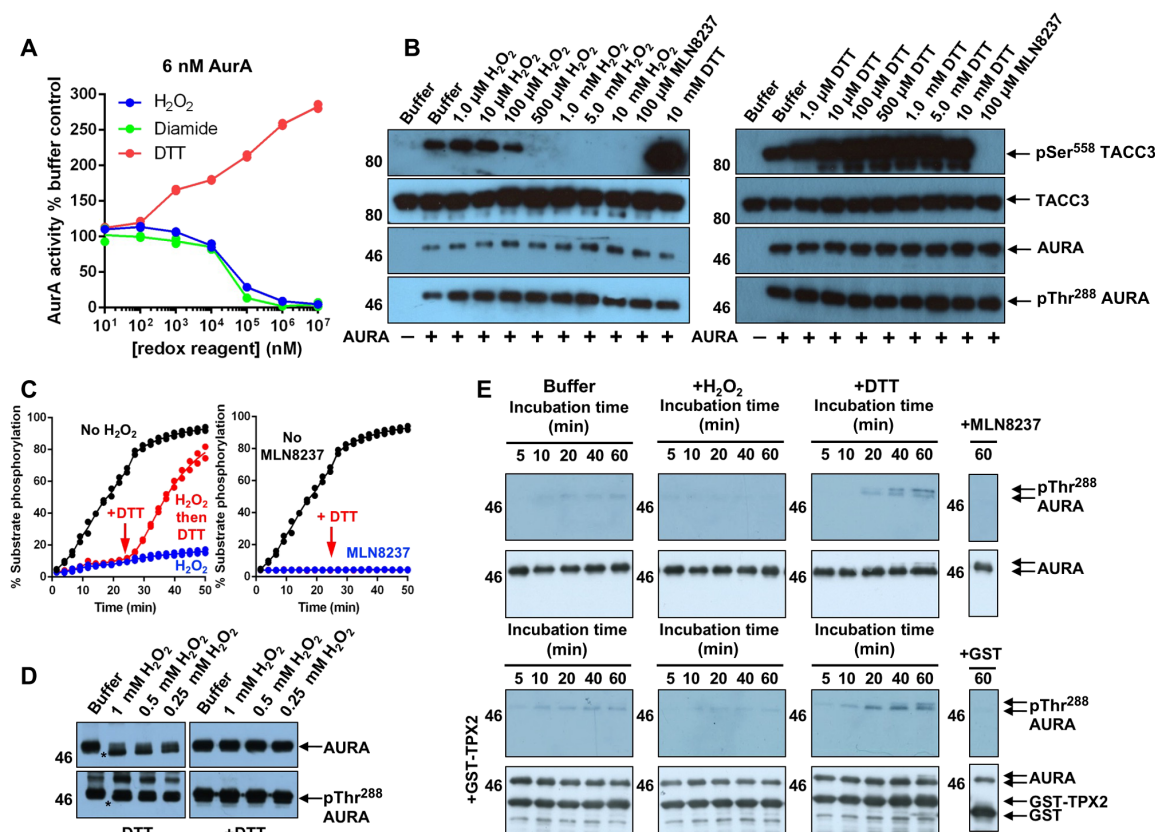


Fig. 1. Redox-dependent regulation of Aurora A activity in vitro. (A) Dose-response curves for DTT (red), H₂O₂ (blue), and diamide (green) with recombinant Aurora A (AurA). Phosphorylation of the fluorescent peptide substrate was measured after 30-min assay time. Data are representative of *N* = 3 biological replicates. (B) Immunoblot of an in vitro kinase assay using recombinant GST-TACC3 as substrate for Aurora A (3 ng), which was preincubated with the indicated concentrations of H₂O₂, DTT, or the Aurora A-specific inhibitor MLN8237 for 30 min at 20°C. (C) Real-time phosphorylation of a fluorescent peptide substrate by Aurora A in the presence (blue) or absence (black) of 1 mM H₂O₂ (left) or 10 μM MLN8237 (right). After 25 min, reactions were supplemented (where indicated) with 2 mM DTT (red). Data from duplicate independent experiments are shown. (D) Immunoblot of Aurora A (0.5 μg) after incubation with the indicated concentrations of H₂O₂ for 10 min at 20°C and analyzed by nonreducing (left) or reducing SDS-PAGE. Asterisks denote the reversibly oxidized species. (E) Immunoblotting of time-dependent Aurora A autophosphorylation at Thr²⁸⁸ in the presence or absence of GST-TPX2, H₂O₂, or DTT.

from Thr²⁸⁸. Accumulation of pThr²⁸⁸ was assessed by immunoblotting after the addition of Mg-ATP in the presence and absence of the known allosteric activator TPX2. Under standard assay conditions, Aurora A autophosphorylation was extremely slow, and only trace amounts of pThr²⁸⁸ Aurora A were detected after 60 min (Fig. 1E). The inclusion of DTT and/or TPX2 markedly increased the rate of Aurora A autophosphorylation, whereas no phosphorylation was detected in the presence of H₂O₂, even in the presence of TPX2 (Fig. 1E). These data confirm that, although peroxide treatment does not lead to loss of Thr²⁸⁸ phosphorylation in phosphorylated Aurora A, reducing conditions are required to stimulate efficient autoactivation of the unphosphorylated “ground-state” form of the enzyme in vitro.

Identification of Cys²⁹⁰ as the site of Aurora A redox regulation

The reversible oxidative modification of signaling proteins is associated with oxidation of the sulfur-containing amino acids cysteine and methionine, with the initial oxidation of a specific cysteine thiol generating a reversible sulfenyl (SOH) derivative (fig. S1) (62). To investigate the presence of Cys-SOH in Aurora A, we exploited an

antibody that detects SOH or sulfenamides that have been selectively and covalently derivatized with dimedone (5, 6, 11, 63). Sulfenylated Aurora A was readily detected (Fig. 2A), with the signal increasing progressively after exposure to increasing concentrations of H₂O₂ (Fig. 2B). Incubation of Aurora A with DTT markedly reduced dimedone labeling (Fig. 2B), consistent with the regeneration of Cys thiols, which are refractory to dimedone adduct formation. No labeling of the protein was detected in the absence of dimedone, confirming antibody specificity (Fig. 2A).

To identify potential redox-sensitive Aurora A residues, we used the bioinformatics tool Cy-preds (64), which highlighted the surface residue Cys²⁹⁰ as a potential target for oxidative modification of the seven human Aurora A Cys residues. Cys²⁹⁰ is highly conserved and lies within the canonical activation segment, in very close proximity to the regulatory Thr²⁸⁸ side chain. The equivalent Cys in PKA has previously been analyzed in terms of redox regulation, with a role for Cys²⁰⁰ established in vitro (57, 65). To assess whether regulatory oxidative modification of Aurora A could be specifically assigned to Cys²⁹⁰, we generated Aurora A containing a Cys-to-Ala substitution at this position (fig. S4A). When compared to wild-type (WT) Aurora A, incorporation of the C290A mutation had no effect on

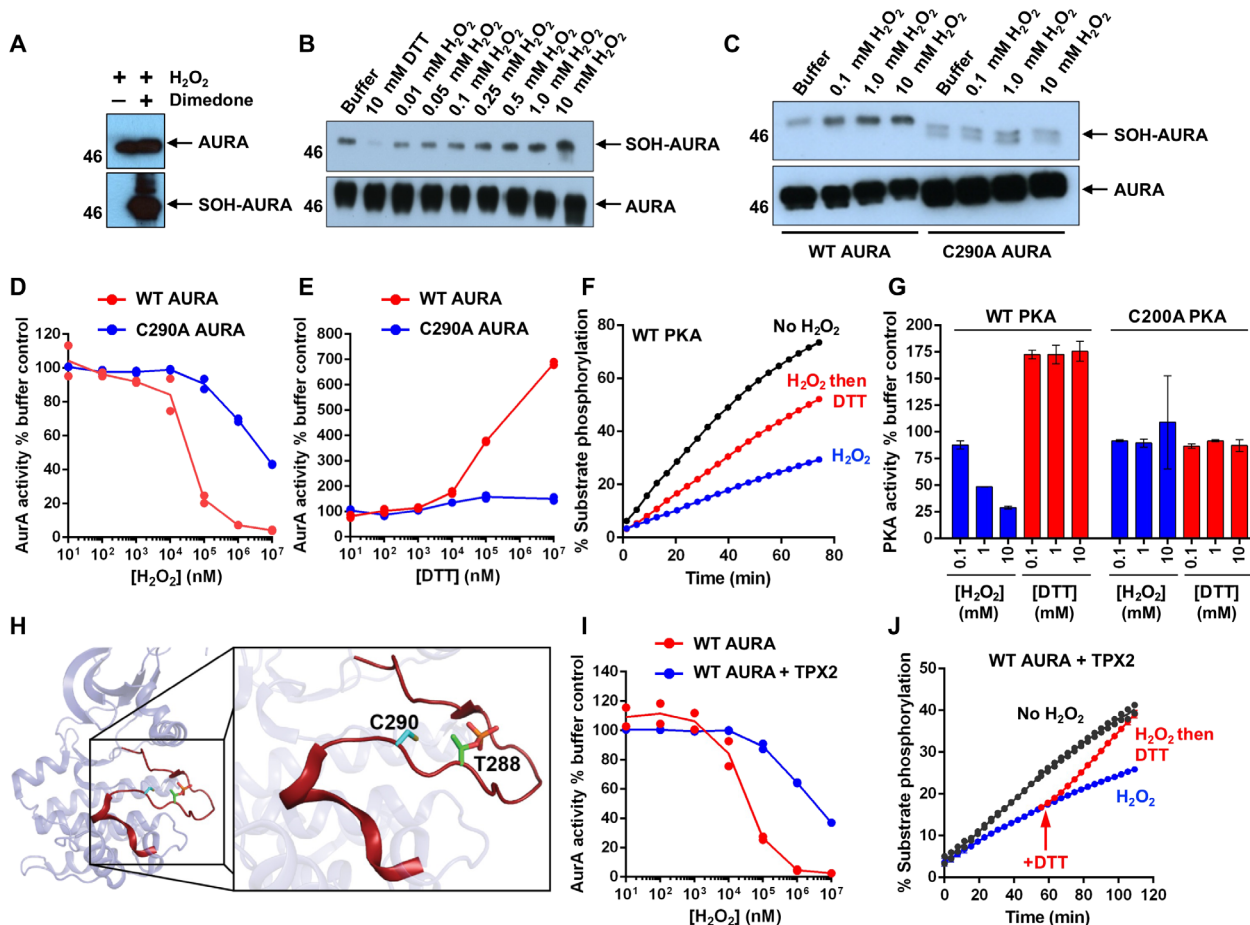


Fig. 2. Conserved Cys²⁹⁰ residue in the Aurora A activation loop is reversibly oxidized in vitro and the effect of TPX2. (A) Detection of reactive cysteine oxidation in Aurora A with an antibody that has specificity toward cysteine sulfenic acids that have been derivatized by dimedone (SOH–Aurora A). (B) Concentration dependent oxidation of Aurora A detected by dimedone. (C) Immunoblotting for total SOH content in Aurora A C290A compared to WT enzyme. (D and E) Comparative analysis of WT (red) and C290A (blue) Aurora A activity in the presence of varying concentrations of either (D) H₂O₂ or (E) DTT and a fluorescent peptide substrate. Aurora A activity was determined after 60-min assay time. (F) Reversible redox regulation of PKA catalytic domain toward a fluorescent peptide substrate. (G) Redox regulation of WT or C200A PKA by the indicated concentration of H₂O₂ or DTT. Data are means ± SD from *N* = 2 biological replicates. (H) Structural disposition of the Aurora A activation segment (red). (I) H₂O₂ dose-response curves of the fluorescent peptide substrate are shown for Aurora A preincubated with or without GST-TPX2 before incubation with the indicated concentration of H₂O₂. Percentage peptide phosphorylation was determined after 40-min assay time. (J) Real-time peptide substrate phosphorylation by Aurora A with GST-TPX2 in the presence (blue) or absence (black) of 1 mM H₂O₂. After 50 min, 2 mM DTT was added to the indicated reactions (red). Assays were started simultaneously with 100 μM ATP. Data for (D) to (F), (I), and (J) are representative of *N* = 3 biological replicates, each performed in duplicate.

protein thermostability ($T_m \sim 40^\circ\text{C}$; fig. S4B) measured by DSF (66, 67) or ΔT_m values induced by ATP or inhibitor (MLN8237) binding (fig. S4C). Furthermore, $K_{M[\text{ATP}]}$ values obtained in peptide-based kinase assays were virtually identical for both kinases, although the C290A mutant exhibited decreased activity ($\sim 50\%$ of WT; fig. S4D). This latter observation is consistent with previous analysis of a C290A Aurora A mutation (68) and emphasizes the potential importance of this residue as a regulatory hotspot within the activation loop.

We next tested whether Cys²⁹⁰ might be prone to oxidation by comparing the H₂O₂-induced sulfenylation of WT and C290A Aurora A in vitro. Immunoblotting that revealed dimedone labeling was greatly diminished in C290A Aurora A compared to WT, indicative of a reduction in the number of Cys residues undergoing sulfenylation (Fig. 2C). Critically, mutation of Cys²⁹⁰ partially protected Aurora A inactivation by H₂O₂ (Fig. 2D). This manifested as an

increase in the half-maximal inhibitory concentration (IC₅₀) of H₂O₂ from $\sim 35 \mu\text{M}$ for WT Aurora A to $\sim 10 \text{ mM}$ for C290A Aurora A. Concomitantly, C290A mutation abolished DTT-dependent activation of Aurora A (Fig. 2E). Our observation that C290A Aurora A was still modified by dimedone, albeit to a lesser extent than for control Aurora A (Fig. 2C), provides evidence for the existence of additional redox-active Cys residues, although their relevance for regulating catalytic activity appears to be secondary to Cys²⁹⁰. Last, we investigated C290A Aurora A–dependent phosphorylation of TACC3, observing that catalytic activity toward this physiological substrate was unaffected by the presence of either reducing or oxidizing agents (fig. S4E). Together, these results confirm that Cys²⁹⁰ plays a central role in a new regulatory mechanism underpinning Aurora A activity in vitro and suggest that this may be a direct result of a switch between oxidized “inactive” and reduced “active” catalytic states.

The reduced C290A phosphotransferase activity (compared to WT Aurora A; fig. S4) suggested that an Ala substitution was not optimal in terms of catalysis. On the basis of its similar size, structure, and hydrophilic properties, Ser is potentially a better-suited (non-redox-sensitive) mimic of this Cys²⁹⁰ residue. However, introduction of a Ser (or Asp) residue at the Cys²⁹⁰ position generated Aurora A that was devoid of Thr²⁸⁸ phosphorylation (fig. S5A), despite no detectable changes in protein stability (as judged by T_m values; fig. S5B) or binding to ATP or MLN8237 (fig. S5C), confirming an inability of the kinase to autophosphorylate and autoactivate. Consistently, both C290S and C290D mutants were catalytically inactive when evaluated in real time (fig. S5D). These observations reveal an extraordinary sensitivity of Aurora A to modest structural perturbations at the Cys²⁹⁰ position and further establishes the potential regulatory role of this conserved site in the activation segment. In agreement with published findings (33, 57, 65), PKA activity was also inhibited in a concentration-dependent manner by H₂O₂, whereas DTT modestly stimulated kinase activity (Fig. 2, F and G). Consistently, the inhibitory effect of H₂O₂ was completely abrogated in the site-specific cysteine mutant PKA C200A (Fig. 2G). Moreover, inhibition of PKA by H₂O₂ was due to the reversible oxidation of a sulfhydryl residue, because activity could be fully restored in real time by subsequent DTT exposure (Fig. 2F).

TPX2 protects Aurora A from inactivating oxidation

In addition to autophosphorylation of Thr²⁸⁸ in the activation loop, which lies directly adjacent to Cys²⁹⁰ (Fig. 2H), Aurora A can be independently activated by allosteric interaction(s) with the spindle assembly factor TPX2 (48, 69–72). Given that binding to TPX2 and phosphorylation of the activation loop are complementary mechanisms for Aurora A activation, we investigated redox regulation of Aurora A in the context of TPX2. First, we considered the effect of redox state on the interaction between Aurora A and TPX2. Aurora A was exposed to increasing concentrations of H₂O₂ or DTT and then evaluated for its ability to interact with glutathione S-transferase (GST)-tagged TPX2. GST pulldown assays revealed that Aurora A remained associated with GST-TPX2 even at the highest concentrations of H₂O₂ and DTT used (fig. S6A). Thus, the redox state of Aurora A had no detectable effect on binding to TPX2 in vitro. Next, we examined the inhibition of Aurora A by H₂O₂ in the presence of TPX2. The phosphorylated activation loop of Aurora A has recently been shown to adopt a range of conformations in solution, only becoming highly ordered in a stable “DFG-in” conformation upon TPX2 binding (72). Furthermore, both “inactive” unphosphorylated and “active” phosphorylated Aurora A adopt similarly well-defined structures upon TPX2 binding, resulting in an increase in kinase activity (49, 72). We found that TPX2 increased the IC₅₀ [H₂O₂] value to >1 mM (Fig. 2I). Moreover, the modest inhibitory effect of H₂O₂ on the TPX2–Aurora A complex could be completely reversed in real time upon addition of DTT (Fig. 2J). Allosteric activation of Aurora A by TPX2 is therefore sufficient to overcome kinase inactivation by oxidation under these conditions. It is possible that the oxidation of Aurora A at Cys²⁹⁰ alters the structural dynamics of the activation loop and stabilizes a less active subpopulation, with activity being recapitulated after binding to, and structural reorganization by, TPX2. This is supported by the observation that C290A Aurora A, which displays lower kinase activity compared to the WT protein, is also strongly activated by TPX2 binding but, unlike WT Aurora A, remains resistant to inhibition by H₂O₂ when TPX2

bound (fig. S6, B and C). Activities of WT and C290A Aurora A were unaffected by GST (fig. S6C). Furthermore, C290S (but not C290D) Aurora A, which lacks kinase activity (and phosphorylation at Thr²⁸⁸) when evaluated in isolation, was partially activated in the presence of TPX2 (but not DTT alone) in a peptide-based kinase assay and also displayed clear phosphotransferase activity toward TACC3 protein (fig. S6, D and E).

Aurora A can also be activated by glutathionylation on Cys²⁹⁰

Sulfenylated cysteines are susceptible to further, irreversible, oxidation. In vivo, reversibility can be ensured by the formation of a disulfide with a cysteine in glutathione or another protein (fig. S1). We therefore investigated the influence of GSH or GSSG alongside a panel of other redox-active compounds on Aurora A activity. Aurora A activation by the reducing agents DTT, tris(2-carboxyethyl)phosphine (TCEP), and 2-mercaptoethanol (βME) was confirmed by enhanced rates of peptide substrate phosphorylation compared to control assays (Fig. 3A). The inclusion of GSH (or GSSG) in the assay also induced a measurable increase in activity (Fig. 3A). This increased Aurora A activity is in contrast to PKA, which is reported to be inhibited by GSH (57). Consistently, C290A Aurora A was more resistant to activation by these reducing agents (Fig. 3B). In addition, in contrast to WT Aurora A, which demonstrated concentration-dependent activation by GSH, C290A Aurora A only exhibited modest increases (~1.5-fold) in activity at the highest tested GSH concentrations (Fig. 3C). Next, we investigated whether modulation of Aurora A activity was a consequence of mixed disulfide formation between Cys²⁹⁰ and glutathione. To probe for glutathionylation, we used an antibody that specifically reacts to protein-glutathione complexes (Fig. 3D). PKA was included as a positive control because it has previously been shown to be glutathionylated (57). Glutathionylation was readily detected for WT Aurora A incubated with GSSG, but not for the C290A mutant, suggesting that changes in Aurora A activity were a direct result of glutathionylation of this cysteine (Fig. 3D and fig. S7A). However, despite stimulating Aurora A activity, the addition of GSH alone was insufficient to restore the activity of oxidized Aurora A (Fig. 3E), which required reduction by DTT (fig. S7B) or enzymatic deglutathionylation by GRX-1 (fig. S7C) to restore Aurora A catalytic activity. The automatic gain control (AGC) kinase AKT has been shown to be regulated by glutathione-dependent mechanisms (36). To confirm AKT glutathionylation using a real-time assay, we incubated 3-phosphoinositide-dependent protein kinase 1 (PDK1)-phosphorylated S473D AKT with GSH in the presence and absence of H₂O₂. Similar to Aurora A, AKT was covalently modified by glutathione (Fig. 3F). The catalytic activity of AKT was also enhanced several hundred-fold by GSH exposure in the absence of H₂O₂ (fig. S7D). Furthermore, the activity of AKT was rapidly inhibited by oxidation and could be restored by the addition of DTT. Subsequent exposure to GSH did not rescue activity (Fig. 3G), as demonstrated for Aurora A.

Oxidative stresses inhibit Aurora A substrate phosphorylation in human cells

To validate our in vitro findings, we next investigated whether Aurora A activity is redox-regulated in human cells, using the endogenous substrate TACC3 phosphorylation as an intracellular readout for Aurora A activity (73, 74). HeLa cells were initially synchronized with nocodazole and then exposed to H₂O₂ or DTT for 30 min. Western blotting revealed a dose-dependent decrease in

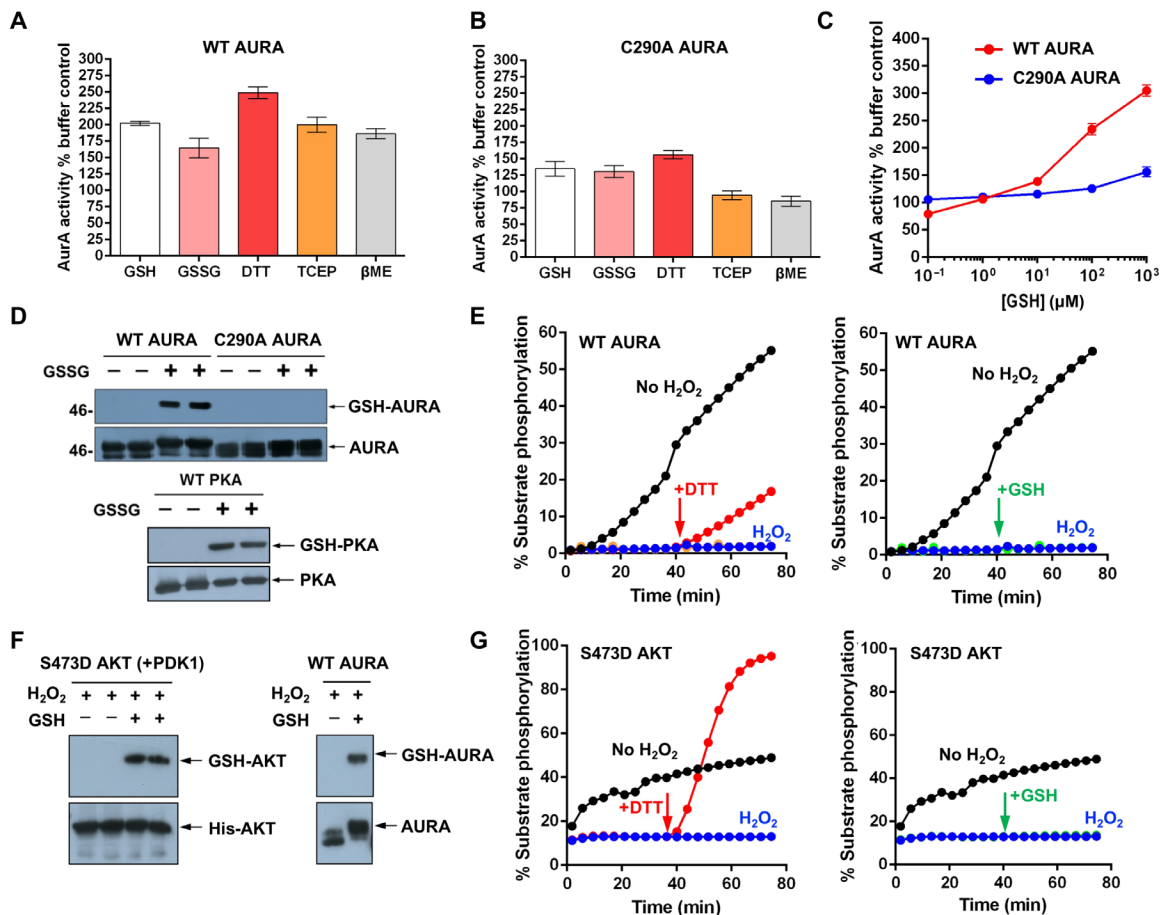


Fig. 3. Aurora A is activated by modification of Cys²⁹⁰. (A and B) Redox-dependent activation of (A) WT or (B) C290A Aurora A by a panel of reducing agents (1 mM) using a fluorescent peptide substrate. Activity was calculated after 40-min assay time. Data are means \pm SD from $N = 2$ biological replicates. (C) Dose-response curves for GSH. The activity of WT and C290A Aurora A was monitored in the presence of increasing concentrations of GSH. The percentage of peptide phosphorylation was determined after 40-min assay time. Data are means \pm SD from $N = 2$ biological replicates. (D) Immunoblotting of in vitro glutathionylation of Aurora A at Cys²⁹⁰. Data from two independent experiments are shown. PKA (1 μ g) was also included as a positive control. (E) In vitro Aurora A activity was assayed in real time using a peptide substrate in the presence or absence of 1 mM H₂O₂ for 50 min, and reactions were supplemented (where indicated) with 2 mM DTT (left) or GSH (right). (F) Immunoblotting of in vitro glutathionylation of AKT. One microgram of active AKT was incubated with 100 μ M H₂O₂ for 10 min before the application of 1 mM GSH (30 min at 20°C). Data from two independent experiments are shown. Aurora A was used as a positive control. (G) In vitro activated AKT activity was monitored in real time in the presence or absence of 1 mM H₂O₂ for 40 min before the addition of 2 mM DTT (left) or GSH (right). Data in (E) and (G) are representative of $N = 2$ biological replicates.

TACC3 phosphorylation at Ser⁵⁵⁸ in cells treated with H₂O₂ compared both to control cells and to those treated with DTT alone (Fig. 4, A and B). As expected, cells incubated with the Aurora A inhibitor MLN8237 demonstrated complete loss of TACC3 phosphorylation (Fig. 4A), whereas nocodazole exposure alone, which has recently been shown to enhance the oxidation of Cys residues (5), did not lead to net Aurora A inhibition. We next determined the effects of the cell-permeable oxidant diamide (56). The extent of TACC3 phosphorylation was inversely proportional to the diamide concentration, analogous to observations with H₂O₂ (Fig. 4C). Menadione is a quinone oxidant that stimulates rapid generation of cellular ROS through redox cycling (75). Menadione exposure also caused a concentration-dependent inhibition of TACC3 phosphorylation (Fig. 4D). Aurora A protein levels were not affected by H₂O₂, diamide, or menadione, eliminating the possibility that kinase degradation was related to reduced TACC3 phosphorylation (Fig. 4, A to D). Last, we investigated the effect of chronic oxidative stress on Aurora

A activity. Glucose oxidase (GO) was added to nocodazole-containing culture medium at a nontoxic concentration (2 U/ml) to facilitate the generation of peroxide. At this level of enzyme activity, GO is reported to generate intracellular steady-state levels of H₂O₂ of 1 to 2 μ M (76–78); here, GO resulted in a time-dependent decrease in TACC3 phosphorylation (Fig. 4E). To evaluate the physiological relevance of Aurora A redox regulation as a signaling mechanism, we also investigated the reversibility of inactivation. Cells were exposed to H₂O₂ before incubation with DTT or the cellular antioxidants GSH and *N*-acetyl-L-cysteine (NAC). Under these conditions, TACC3 phosphorylation was restored to basal levels by both GSH and NAC, presumably due to ROS scavenging (Fig. 4F). However, in the presence of H₂O₂, DTT was unable to rescue TACC3 phosphorylation. The inability of DTT to restore Aurora A activity in vivo likely reflects cellular effects on the oxidation state of endoplasmic reticulum proteins and subsequent enhanced ROS generation as part of the unfolded protein response (79).

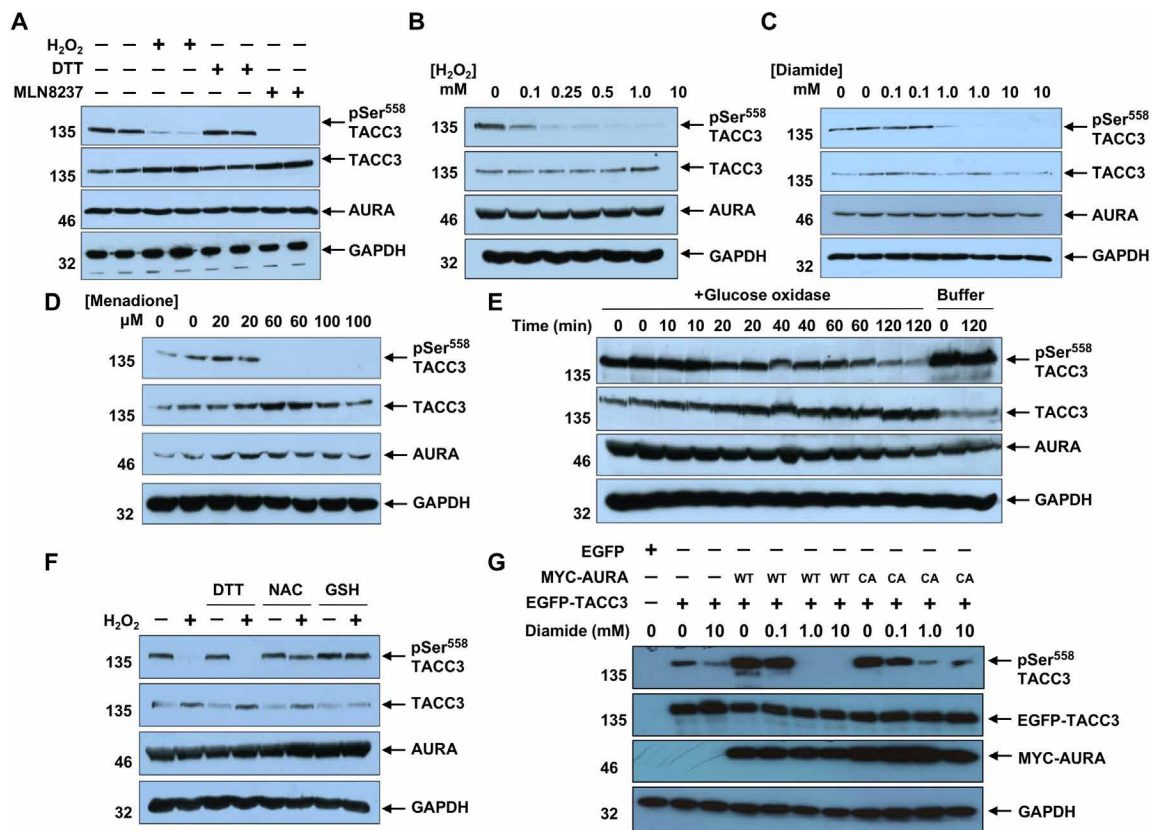


Fig. 4. Oxidative stress inhibits endogenous Aurora A activity in human cells. (A) Immunoblotting for Aurora A–dependent phosphorylation of TACC3 (pTACC3) in HeLa cells either untreated or treated with 10 mM H₂O₂ or 1 μM MLN8237 for 30 min. (B) Immunoblotting analysis of pTACC3 in HeLa cells incubated with the indicated concentration of H₂O₂ for 30 min. Blot is representative of two independent experiments. (C and D) Analysis of pTACC3 in HeLa cells incubated with the indicated concentration of the diamide for 30 min (C) or menadione for 60 min (D). (E) Loss of pTACC3 in HeLa cells exposed to glucose oxidase (GO). (F) Immunoblots of HeLa cells treated with 10 mM H₂O₂ for 10 min before the addition of fresh culture medium containing 10 mM DTT, NAC, or GSH (or buffer control). Cells were then cultured for an additional 20 min before the extraction of whole cell lysates. In all experiments described here, HeLa cells had been blocked in mitosis by nocodazole. (G) Immunoblots showing phosphorylation of GFP-TACC3 by wild-type (WT) and C290A (CA) Myc–Aurora A in cotransfected HeLa cells. EGFP transfections were used as a negative control. In all panels, representative data of two biological replicates are shown.

Next, we analyzed Cys²⁹⁰-based regulation in Aurora A. HeLa cells were transiently cotransfected with green fluorescent protein (GFP)-tagged TACC3 in the presence or absence of either WT or C290A Myc-tagged Aurora A and synchronized with nocodazole to activate Aurora A. GFP-tagged TACC3 became phosphorylated at Ser⁵⁵⁸ by endogenous Aurora A after nocodazole treatment, with a concomitant decrease in phosphorylation at this site in the presence of diamide (Fig. 4G). Transient overexpression of either WT or C290A Myc-tagged Aurora A also led to an increase in GFP-TACC3 phosphorylation at Ser⁵⁵⁸. We detected a diamide-induced, dose-dependent decrease in GFP-TACC3 phosphorylation cotransfected with WT Aurora A, consistent with the inhibition of Aurora A by oxidation. In contrast, the inhibitory effect of diamide on GFP-TACC3 phosphorylation was blunted in cells expressing C290A Aurora A (Fig. 4G). Together, these data suggest that Cys²⁹⁰ in Aurora A is important for inhibition of its kinase activity in response to oxidants in cells.

Cys residues are evolutionary conserved in a variety of ePK activation segments

Cys is the second least common amino acid in vertebrate proteomes (80), and although >200,000 Cys residues are present in the human

proteome, they are often conserved in redox “hotspots” (81). Reactive Cys side chains, especially those lying on surface-exposed regions of proteins (64), are often susceptible to redox modification (fig. S1). To investigate the potential generality of Cys-based redox mechanism in protein kinases that have an activation segment, we analyzed >250,000 protein kinase-related sequences, confirming that ~11.5% of ePKs found across the kingdoms of life have the Cys²⁹⁰ equivalent of Aurora A (Fig. 5A). This number reduced to 1.4% of all ePKs when the coconservation of Cys residues at the DFG +2 and “T-loop +2” positions, which individually are the most prevalent in these kinases, was considered side by side (Fig. 5A, bottom). The Cys²⁹⁰-equivalent residue (table S1) was very strongly associated with two of the seven human kinase groups: the AGC kinases and the Ca²⁺/calmodulin-dependent protein kinases (CAMKs) (Fig. 5B), and this pattern was also observed in kinomes from all the kingdoms of life, including model genetic organisms such as fungi (fig. S8, A to E). Cys residues are encoded locally in eukaryotic kinomes at every possible position within the conserved activation segment, between the DFG and APE motifs (fig. S8F and table S2). However, analysis of all canonical human kinases and pseudo-kinases demonstrated that most of the Cys-containing kinases belong to families encoding Ser/Thr kinases, notably stress-activated protein kinase kinases such as

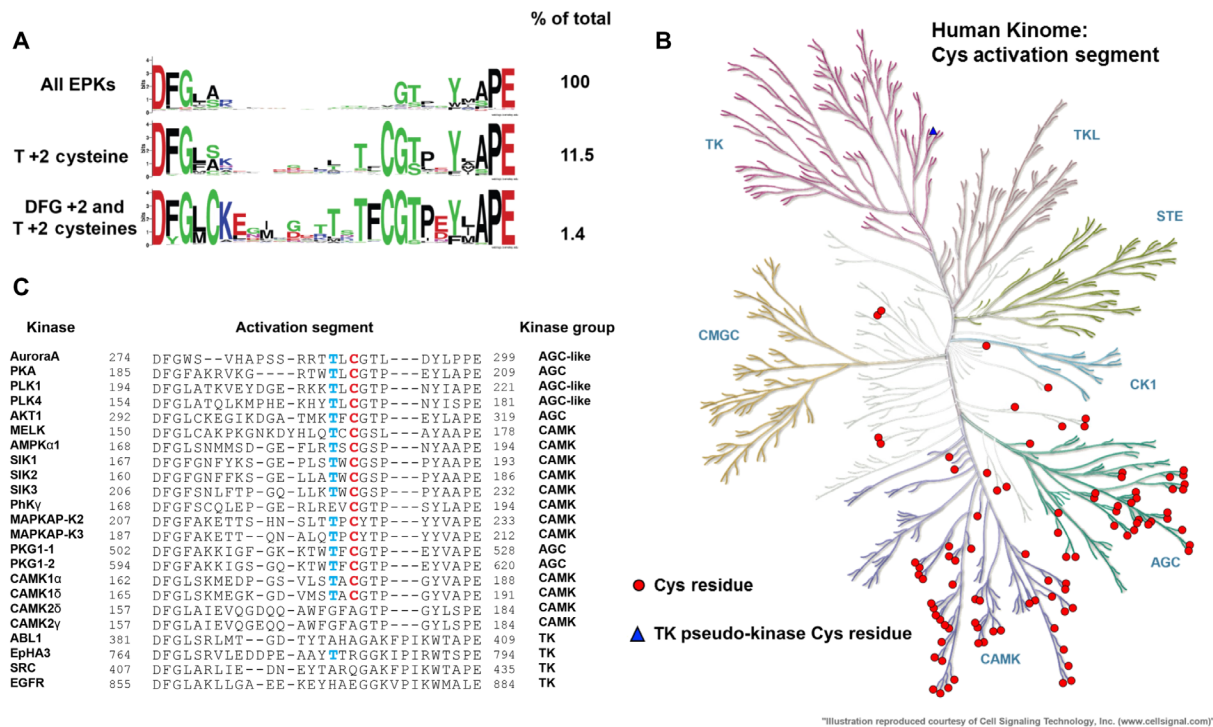


Fig. 5. Bioinformatics analysis of Aurora A Cys²⁹⁰ equivalent in all ePKs. (A) Analysis of ePKs, centered on the activation segment between the canonical DFG and APE motifs. The amino acid distribution (percentage of all kinases) is shown on right, data presented as HMM (hidden Markov models) Sequence Logos. (B) Human Kinome dendrogram, showing highly skewed distribution of kinases containing a Cys residue at the T-loop +2 residue in AGC and CAMK groups. (C) Activation segment alignment of human kinases analyzed in this study.

MAPK-activated protein kinase 2/3 (MAPKAP-K2/3), MAPK kinase kinase 3 (MKK3), MKK4, MKK6, and MKK7 and Cys-rich pseudo-kinases such as Tribbles 1 to Tribbles 3 (67), all of which have a conserved Cys at the DFG +4 position (82).

The conserved redox-sensitive cysteine is important for the in vivo activities of fission yeast Pka1 and MAPK-activated kinase, Srk1

Having established that Cys²⁹⁰ is important for the activity and redox sensitivity of human Aurora A kinase, we investigated whether the equivalent Cys was important for the in vivo activity of well-characterized examples of the AGC and CAMK groups in the fission yeast *Schizosaccharomyces pombe*, by studying the single PKA catalytic subunit (Pka1) and the MAPK-activated kinase, Srk1, which is a homolog of human MAPKAP-K2 (83, 84).

Initially, we examined whether Cys³⁵⁸, equivalent to Cys²⁹⁰ in human PKA (Figs. 5C and 6A), was important for the activity of the single catalytic subunit of PKA, termed Pka1, by ectopically expressing WT Pka1 or Pka1 in which Cys³⁵⁸ was substituted with Ser (C358S) or Ala (C358A) in $\Delta pka1$ mutant cells. Immunoblotting with antibodies that recognize cellular phosphorylated PKA substrates (85) detected fewer bands in *pka1* mutant cells than WT (*pka1*⁺) cells, confirming that these bands represented substrates of Pka1. High-level ectopic expression of WT Pka1 restored the missing phosphorylated Pka1 substrate signals, increasing their intensity to WT levels and confirming that Pka1 substrate phosphorylation was restored. In contrast, despite similar expression (Fig. 6B), Pka1^{C358S} and Pka1^{C358A} only partially restored Pka1 activity, based on com-

parison with a Pka1 phosphospecific substrate antibody (Fig. 6B). Pka1 has a number of well-established roles in regulating *S. pombe* growth and survival under stress conditions. For example, $\Delta pka1$ mutant cells are unable to adapt and grow under high salt conditions (Fig. 6C) (86). We therefore examined whether Cys³⁵⁸ in Pka1 was important for adaptation to high salt by comparing the growth of $\Delta pka1$ mutant cells expressing WT Pka1, Pka1^{C358S}, or Pka1^{C358A} on plates containing 1 M KCl. Consistent with Cys³⁵⁸ playing an important role in Pka1 activity, neither Pka1^{C358S} nor Pka1^{C358A} was able to restore growth to the same extent as WT Pka1 (Fig. 6C).

Next, we examined whether the equivalent conserved Cys (Cys³²⁴) was important for the activity of the MAPK-activated kinase Srk1. Srk1 expression delays entry to mitosis by phosphorylating the dual-specificity phosphatase CDC25 (87). Accordingly, in cells ectopically overexpressing Srk1 from a multicopy plasmid, CDC25 is excluded from the nucleus, causing a G₂ delay that results in some substantially elongated cells (Fig. 6D) and increases the mean length of cells at mitosis (Fig. 6D). In contrast, despite similar expression levels (Fig. 6E), ectopic expression of Srk1^{C324S} or Srk1^{C324A} produced a much more modest increase in cell length (Fig. 6D) and failed to block nuclear localization of CDC25 (Fig. 6F). This permits us to conclude that Cys³²⁴ in Srk1 is important for the in vivo activity of Srk1 in delaying mitotic entry by phosphorylating CDC25 (87). Together, these data establish that the T-loop +2 Cys plays an important role in the activity of both these kinases, raising the possibility that redox modification of this cysteine may regulate the roles of these kinases in controlling cell division and stress resistance.

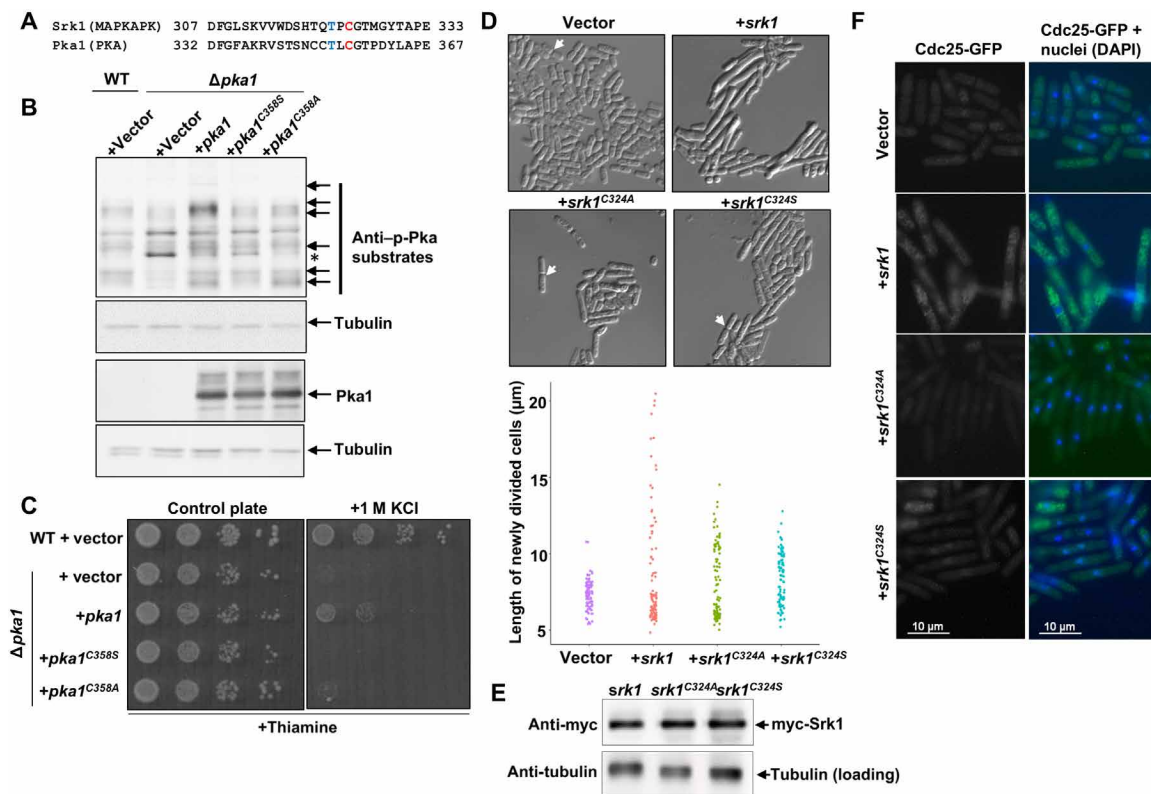


Fig. 6. Evaluating the regulatory importance of activation segment cysteine residues in *S. pombe* PKA (Pka1) and MAPKAP-K2 (Srkl1). (A) Sequence comparison between *S. pombe* Pka1 and MAPKAP-K2/Srkl1, showing the presence of the conserved activation loop Cys residue; Cys³⁵⁸ in Pka1 and Cys³²⁴ in Srkl1. (B and C) Analysis of Pka1-dependent phosphorylated substrates and cell growth analysis on control medium and medium containing 1 M KCl. PKA substrate phosphorylation was detected using phospho-specific PKA substrate (RRXpS/pT) antibodies in exponentially growing wild-type (WT; JY333) or $\Delta pka1$ (JX384) *S. pombe* expressing pk-tagged wild-type Pka1, Pka1^{C358S}, or Pka1^{C358A} compared with vector control (Rep41pkc). Asterisk indicates an unknown immunoreactive band. (D and E) Analysis of mitotic entry (as increasing cell length) in exponentially growing wild-type *S. pombe* (AD38) expressing wild-type Myc-tagged Srkl1, Srkl1^{C324S}, or Srkl1^{C324A} compared with vector control (Rep41HM). The graph shows the cell length of >94 newly divided cells, such as those indicated by arrows in images (D). Similar expression of wild-type Myc-tagged Srkl1^{C324S} and Srkl1^{C324A} Srkl1 proteins, relative to a tubulin loading control, was confirmed (E). (F) Analysis of Cdc25-GFP-expressing cells (KGY4337) coexpressing wild-type Srkl1, Srkl1^{C324S}, or Srkl1^{C324A}, compared with vector control (Rep41HM) using fluorescence microscopy. Right: Cells were stained with DAPI to visualize DNA (blue). Scale bars, 10 μ m. In all panels, data are representative of $N = 2$ independent experiments and $N = 3$ in (C).

Analysis of human MAPKAP-K2 and Polo-like kinases

To further investigate the importance of the T-loop +2 Cys in redox regulation, we analyzed a variety of T-loop +2 Cys-containing kinases (Fig. 5C), beginning with MAPKAP-K2, Polo-like kinase 1 (PLK1), and PLK4, which were assayed using the real-time microfluidic kinase assay developed for Aurora A but modified to include kinase-specific peptide substrate sequences (table S2).

Recombinant, bacterially expressed, GST-tagged MAPKAP-K2 was activated by DTT, inhibited by peroxide, and reactivated by subsequent exposure to DTT (Fig. 7A). To evaluate this effect in MAPKAP-K2 purified from human cells, we generated 3C protease-cleavable MYC-tagged constructs of WT and C244A MAPKAP-K2 and purified them from human embryonic kidney (HEK) 293T cells (Fig. 7B). After immunoprecipitation, bound proteins were eluted using 3C protease and then assayed in real time in the presence of DTT or diamide. The inhibitory effect of diamide on WT MAPKAP-K2 activity was reduced in the C244A MAPKAP-K2 mutant (Fig. 7C), confirming that this Cys residue is required for full oxidative inhibition of the kinase.

The Aurora kinases and PLKs both perform complementary mitotic roles (88). The PLK family is stringently regulated multifaceted

modulators of mitosis and cytokinesis (89), and the close regulatory relationship between PLK1 and Aurora A in mitosis (52, 90) led us to investigate potential redox regulation for PLK1 and PLK4. (91). We demonstrated the dose-dependent activation and inhibition of bacterially expressed, truncated PLK1 by DTT and H₂O₂, respectively (Fig. 7D), and inhibitory oxidation was reversed in real time by subsequent exposure to DTT (Fig. 7E). However, mutation of the T-loop +2 Cys residue of truncated PLK1 (amino acids 1 to 361) purified from *Escherichia coli* resulted in a kinase that was catalytically inactive, which prohibited further analysis. We therefore immunoprecipitated full-length PLK1 from human cells (Fig. 7F) and compared WT and C212A PLK1 responses using the same substrate peptide (Fig. 7G). Consistently, full-length PLK1 was inhibited by both diamide and the inhibitor BI2536 (Fig. 7G). Not only was full-length C212A PLK1 catalytically active, but peptide phosphorylation was also preserved under experimental oxidizing conditions that led to the complete inactivation of WT PLK1 (Fig. 7G). Next, we evaluated the related Ser/Thr kinase PLK4, a “master” centrosomal kinase (92, 93), which has a conserved Cys residue (Cys¹⁷²), +2 residues from the T-loop autophosphorylation site (Thr¹⁷⁰). Consistently, PLK4 was reversibly inhibited by H₂O₂, and activity was both rescued

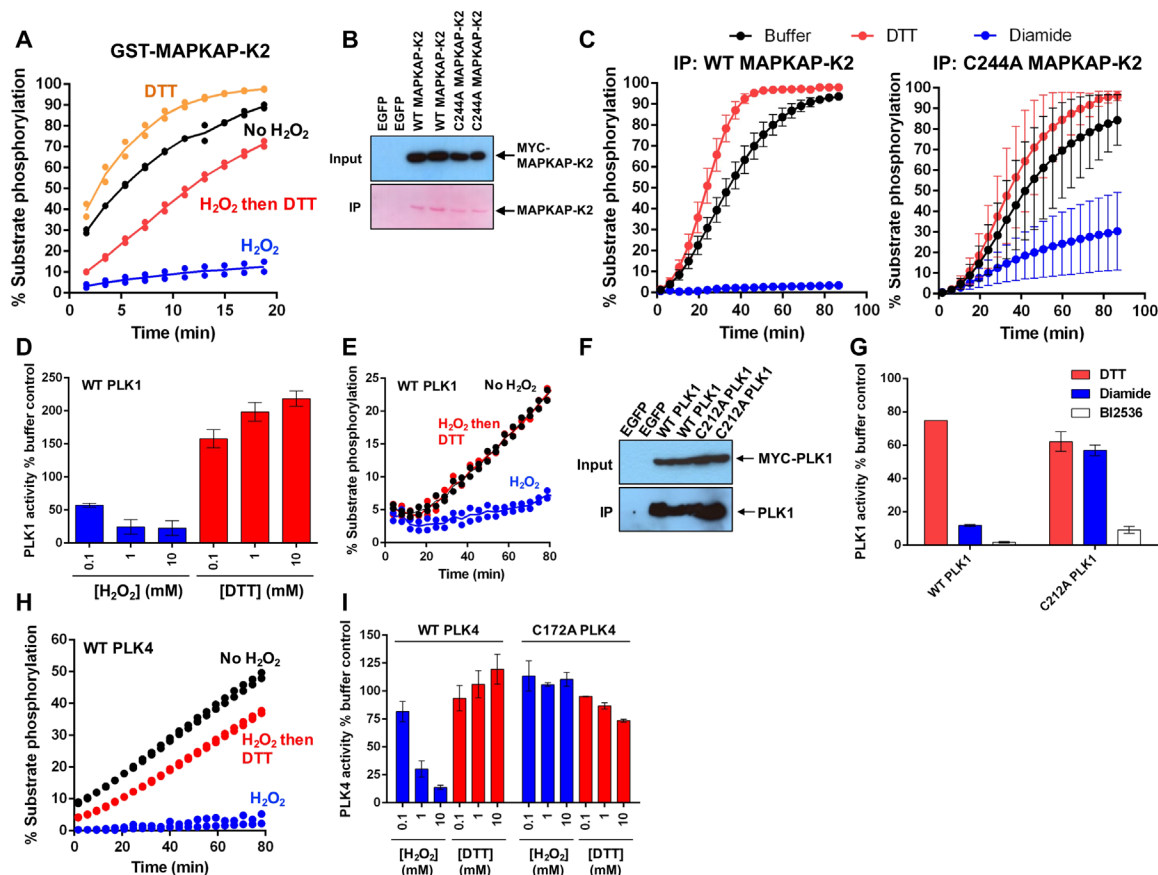


Fig. 7. Analysis of redox regulation in human MAPKAP-K2, PLK1, and PLK4. (A) In vitro peptide assay showing reversible redox regulation of GST-MAPKAP-K2. (B) Immunoprecipitations (IP) of N-terminal Myc-tagged WT and C244A MAPKAP-K2 from HEK 293T cells from two independent transfection experiments. Overexpression of Myc-MAPKAP-K2 in lysates was detected using an antibody for Myc-tagged proteins (top), and purified MAPKAP-K2 was detected by Western blotting, followed by Ponceau staining (bottom). EGFP transfections were used as a negative control. (C) The activity of immunoprecipitated WT and C244A MAPKAP-K2 was measured in the presence of 1 mM DTT (red), 1 mM diamide (blue), or buffer control (black). MAPKAP-K2-dependent phosphorylation of fluorescent substrate peptide was monitored in real time. Data are means \pm SD of $N = 2$ independent immunoprecipitation experiments, each assayed in duplicate. Equal volumes of eluted protein were used in each assay for WT and mutant proteins. (D) In vitro peptide-based kinase assay assessing redox regulation of recombinant GST-PLK1 catalytic domain in the presence of the indicated concentration of H_2O_2 or DTT. Data are means \pm SD from $N = 2$ biological replicates performed in duplicate. (E) Reversible redox regulation of PLK1. (F) Immunoprecipitations of N-terminal Myc-tagged WT and C212A PLK1 from HEK 293T cells from two independent transfections. Overexpressed Myc-PLK1 was detected in lysates using anti-Myc antibody (top), and purified PLK1 was confirmed using anti-PLK1 antibody (bottom). EGFP control data are also shown. (G) The activity of immunoprecipitated WT and C212A PLK1 was measured in the presence of 1 mM DTT (red), 1 mM diamide (blue), or 100 μ M of the PLK-specific inhibitor BI2536 (black). Activity was calculated relative to a control (buffer only) after 2-hour assay time. Data are means \pm SD of two independent experiments. (H) Real-time reversible redox regulation of WT His-PLK4 catalytic domain. (I) In vitro redox regulation of WT and C172A His-PLK4. Data are means \pm SD from $N = 2$ biological replicates. Data in (A), (E), and (H) are representative of $N = 2$ independent experiments from in vitro peptide assays.

and stimulated under reducing conditions (Fig. 7H). Moreover, C172A PLK4 was refractory to inhibition by oxidation, confirming the role of this Cys residue as a central regulator of catalytic activity (Fig. 7I). Supporting the evolutionary relevance of these previously unknown findings, analysis of homologous kinases demonstrated that the Cys²⁹⁰ equivalent was conserved across all known eukaryotic Aurora, PKA, and PLKs (fig. S8, A to E).

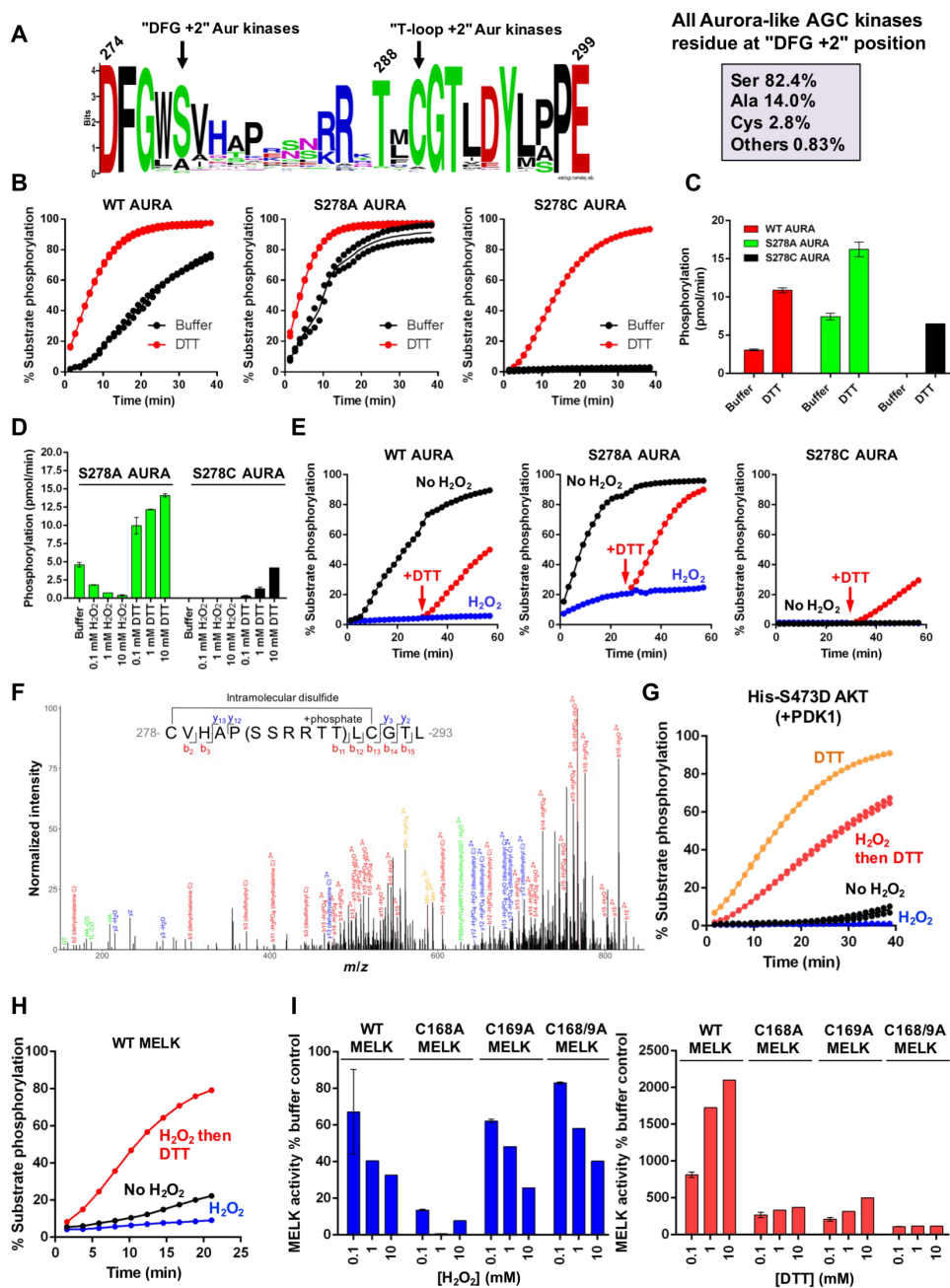
The presence of a Cys at residue DFG +2 converts Aurora A into an enzyme that requires DTT for activity

To help understand the mechanism of redox regulation in Aurora A, we investigated the DFG +2 amino acid in Aurora A, which is a Ser or Ala in all multicellular vertebrates (Fig. 8A) but a Cys in many apicomplexan and fungal species. We first analyzed purified

Aurora A DFG +2 mutants side by side (fig. S10A). The presence of an Ala residue at position 278 did not change thermal stability (fig. S10, B and C) or alter the redox-sensitive catalytic output of Aurora A (Fig. 7B, left and middle), whereas the introduction of a Cys residue had a marked effect, with S278C exhibiting a ΔT_m of +5°C (fig. S10, B and C) and an absolute requirement for DTT to generate catalytic activity [Fig. 8, B (right), C, and D]. Similar to WT Aurora A, S278A was still reversibly inhibited by peroxide and activated by DTT, in contrast to S278C, which was inactive until DTT was spiked into the assay (Fig. 8E, right). Immunoblotting confirmed that S278C contained lower levels of Thr²⁸⁸ autophosphorylation after purification (fig. S10D), which likely contributes to its lower activity but which cannot explain the marked, and instantaneous, effect of DTT on kinase activity. We predicted that the obligate requirement for DTT

Fig. 8. Redox response of an engineered Ser/Thr kinase: A DFG+2 Cys residue generates an obligate DTT requirement for catalytic activity in Aurora A.

(A) Activation segment amino acid conservation in 2285 Aurora kinase-like AGC family members from diverse eukaryotic kinomes. Human Aurora A sequence annotation is used to highlight Asp²⁷⁴ and Glu²⁹⁹, which encompass the activation segment. The T-loop residue (Thr²⁸⁸) is highlighted. The height of the letters indicates the relative frequency of the amino acid at each position. (B) Real-time enzyme activity of Aurora A and DFG+2 point mutants, S278A and S278C toward fluorescent peptide substrate measured in the presence (red) or absence (black) of 10 mM DTT. Two replicate experiments are shown. (C) Comparison of WT (red bars), S278A (green bars), and S278C (black bars) Aurora A catalytic activity (picomoles of phosphate incorporated into peptide substrate per minute) after 10 min. Data are means \pm SD of two replicates, each assayed in duplicate. (D) Direct comparison of Aurora A S278A (green bars) and S278C (black bars) catalytic activity in the presence of the indicated concentration of H₂O₂ or DTT. Data are presented as mean rate of peptide phosphorylation (picomoles of phosphate/min) \pm SD of two replicates, each assayed in duplicate. (E) Real-time reversible redox regulation of Aurora A DFG+2 mutants in vitro. Aurora A activity was monitored in the presence (blue) or absence (black) of 2 mM H₂O₂. After 30 min, reactions were supplemented (where indicated) with 5 mM DTT (red). (F) Intramolecular disulfide bonding in a S278C mutant to Cys²⁹⁰ in the active site of Aurora A. MS/MS spectrum of the triply charged peptide ion of *m/z* 593.9391, fragmented using HCD. Peptide sequence is displayed with the annotated HCD product ions labeled, including the position of the Cys¹ (amino acid 278)–Cys¹³ (amino acid 290) disulfide bond. HCD resulted in peptide backbone fragmentation and cleavage of the disulfide bond (producing dehydroalanine or disulfhydryl cysteine with mass shifts of -33.987 and $+31.971$ amu, respectively (134). a/b ions (red), y ions (blue), internal ions (green), and precursor derived product ions (orange) are annotated, including charge state and neutral losses. MS1 mass is equivalent to a singly phosphorylated peptide; however, the specific site(s) of phosphorylation could not be localized in the spectrum. (G) Real-time reversible redox regulation of active AKT in vitro. Data are representative of *N* = 3 experimental repeats. (H) Real-time reversible redox regulation of active MELK in vitro. Data are representative of *N* = 3 experimental repeats. (I) Redox regulation of MELK and mutants. WT and activation loop Cys mutants were assayed with H₂O₂ (left) or DTT (right) in the presence of a specific peptide substrate. For all panels, data are means \pm SD from *N* = 2 biological replicates performed in duplicate.



to activate S278C Aurora A was due to the presence of an inhibitory intermolecular disulfide bond forming between Cys²⁹⁰ and the newly introduced Cys²⁷⁸, in a manner analogous to other DFG+2 cysteine containing kinases that also have cysteines at the T-loop +2 position, such as AKT and MELK (see below). This hypothesis was confirmed by inspection of peptides derived from S278C Aurora A by liquid chromatography–tandem mass spectrometry (LC-MS/MS), which revealed the presence of a DTT-reversible intramolecular

disulfide bond formed between Cys²⁷⁸ and Cys²⁹⁰ that was absent in WT Aurora A (Fig. 8F).

AKT and MELK require the presence of a reducing agent for catalysis

Next, we confirmed that the inclusion of DTT in the buffer enhanced AKT catalytic activity several hundred-fold (Fig. 8G). In contrast, oxidation completely prevented AKT-dependent substrate peptide

phosphorylation, although activity was restored, or even enhanced, by subsequent DTT exposure, similar to our findings with S278C Aurora A. Consistently, both of these proteins contain spatially related Cys residues in the activation segment (Figs. 5A and 8A). MELK is a member of the CAMK kinase grouping and is closely related to the adenosine 5'-monophosphate-activated protein kinase (AMPK)-related kinases (94, 95). Redox regulation of MELK has previously been reported, although precise regulatory mechanisms remain unclear (96). The activation segment of MELK contains two consecutive Cys residues (Fig. 5C), one of which might form an intramolecular disulfide bond with a Cys supplied by the DFG +2 Cys, as previously described for an inhibited oxidized state of AKT (36, 97). MELK exhibited very low activity in the absence of DTT, with activity increasing several hundred-fold after inclusion of DTT in the assay (Fig. 8, H and I). H₂O₂ inhibited MELK activity in a dose-dependent manner, and DTT-dependent activation was so pronounced that MELK activity rapidly surpassed control levels when DTT was used to “rescue” H₂O₂ inhibition (Fig. 8, H and I). Individual C168A and C169A point mutation blocked DTT-dependent MELK activation, but neither mutation in isolation completely abrogated MELK redox sensitivity, particularly oxidation by peroxide (Fig. 8I). However, combined mutation (C168A/C169A MELK) abolished DTT-dependent activation, and these Cys mutations diminished dimer adduct formation, especially under control conditions in the absence of peroxide (fig. S9, A and B), extending previous findings (96).

Evaluation of redox regulation in a Cys-containing CAMK and AGC kinase panel

To establish generality for a Cys-based mechanism of Ser/Thr kinase regulation, we increased the scope of our analysis to incorporate a panel of protein kinases containing an evolutionary-conserved Cys residue in the T-loop +2 position of the activation segment (Fig. 5C). All enzymes were purified (or supplied) in the presence of 1 mM DTT and assayed in real time using specific peptide substrates. Catalytic activity was quantified in the presence of additional DTT, H₂O₂, or H₂O₂, followed by DTT. The majority of kinases tested (table S3) displayed redox-dependent regulation. Redox analysis of MAPKAP-K3 demonstrated potent inhibition of enzyme by peroxide (Fig. 9A). Consistent with our observations with GST-MAPKAP-K2 (Fig. 7A), DTT also activated and restored activity to peroxide-treated MAPKAP-K3 (Fig. 9A). The removal of the GST tag in the MAPKAP-K3 preparation also eliminates any possibility that the redox regulation of MAPKAP-K2 kinase activity was mediated by the affinity tag (Fig. 7A).

The AMPK holoenzyme complex (composed of α_1 , β_2 , and γ_1 subunits) is a member of the CAMK family and was also inhibited by H₂O₂ in a DTT-reversible manner (Fig. 9B). These findings support a growing body of evidence that ROS participate in the cellular regulation of AMPK activity through Cys modification, including recent proteomic data (98), although the precise mechanism is unknown. Direct activation of AMPK α catalytic subunits in the presence of H₂O₂ has also previously been described (99), whereas inhibition of AMPK α activity through Cys^{130/174} oxidation has also been reported (34). Cys¹⁷⁴ in AMPK α is analogous to Cys²⁹⁰ of Aurora A and is situated two amino acids C-terminal to the Thr¹⁷² phosphorylation site, the critical positive modulator of AMPK activity by “upstream” kinases. The salt-inducible kinases (SIK1 to SIK3) are also members of the AMPK-related family of CAMKs (100), and all contain a T-loop +2 Cys residue. Consistently, purified SIK1 to SIK3 were all

reversibly inhibited after H₂O₂ exposure (Fig. 9, C to E). H₂O₂ was also weakly and reversibly inhibitory toward toward phosphorylase kinase catalytic subunit, PhK γ , a member of the CAMK group (fig. S11A).

PKG belongs to the AGC group of kinases, although its mechanism of regulation is distinct from that of closely related PKA and protein kinase C (PKC) isozymes. However, and in contrast to other T-loop Cys-containing AGC kinases tested (including PKA and AKT), there was no evidence for oxidative inhibition of the PKG1 splice variants PKG1-1 or PKG1-2, when they were assayed in either the absence, or presence, of guanosine 3',5'-monophosphate (cGMP) (fig. S11, B to E), which is consistent with recent findings (38). In contrast, oxidative modification of PKG1-1 (but not PKG1-2) was previously suggested to result in activation of the kinase in a cGMP-independent manner (31), but we were unable to detect such an effect using our assay system (fig. S11).

CAMK1 has been reported to be inhibited by glutathionylation of Cys¹⁷⁹ in the activation segment (101). Consistently, we found that exposure to peroxide was sufficient to inactivate two isoforms of CAMK1, CAMK1A, and CAMK1D, both of which were assayed in an identical fashion (Fig. 9, F and G). Inactivation is potentially as a consequence of Cys¹⁷⁹ oxidation, but independent of the affinity tag, because GST was proteolytically excised in the CAMK1A sample but still present in CAMK1D. Consistently, DTT exposure reversed H₂O₂-dependent inhibition of both CAMK1 isoforms (Fig. 9, F and G). The related CAMK2 kinases lack an activation segment T-loop +2 Cys residue, but redox regulation of dual-Met residues has been reported to promote CAMK2 activation by stabilizing a calcium/calmodulin-independent active species (102). Consistently, CAMK2G was robustly activated by DTT and inhibited reversibly by H₂O₂ (Fig. 9H), validating a non-Cys activation segment mechanism of redox regulation for this kinase. In contrast, CAMK2D was completely resistant to changes in redox when assayed in the presence of Ca²⁺ and calmodulin (Fig. 9I), demonstrating that neither peroxide nor DTT acts as nonspecific regulatory factors for these recombinant kinases under our experimental conditions. Together, our data suggest that redox regulation is a conserved, reversible mechanism for multiple Ser/Thr kinases in vitro.

Last, we examined redox regulation in Tyr kinases, which with a few exceptions (table S2), does not contain any conserved Cys residues in the activation segment and, as a family, has none at all at the T-loop +2 position (Fig. 5B). The EPHA3 Tyr kinase domain was completely resistant to inhibition or activation by peroxide and DTT, respectively (fig. S12A). ABL also lacks a T-loop Cys residue but is known to be susceptible to alternative modes of redox-dependent regulation (103). Reversible inactivation of ABL by peroxide was also observed in a real-time assay (fig. S12B). We next attempted to sensitize EPHA3 to Cys-based redox regulation by incorporating Cys residues at equivalent positions in the activation segment (Fig. 5C). However, both G784C and a double mutant EPHA3 protein containing G783C and G784C substitutions remained unresponsive to peroxide or DTT (fig. S12, D and E), whereas G783C EPHA3 lacked any detectable phosphotransferase activity (fig. S12C), suggesting that this Gly residue is critical for activity.

DISCUSSION

Aurora A is a redox-sensitive Ser/Thr kinase

In this study, we demonstrate that Aurora A is susceptible to direct reversible, oxidative inactivation in vitro and in cells, by a mechanism

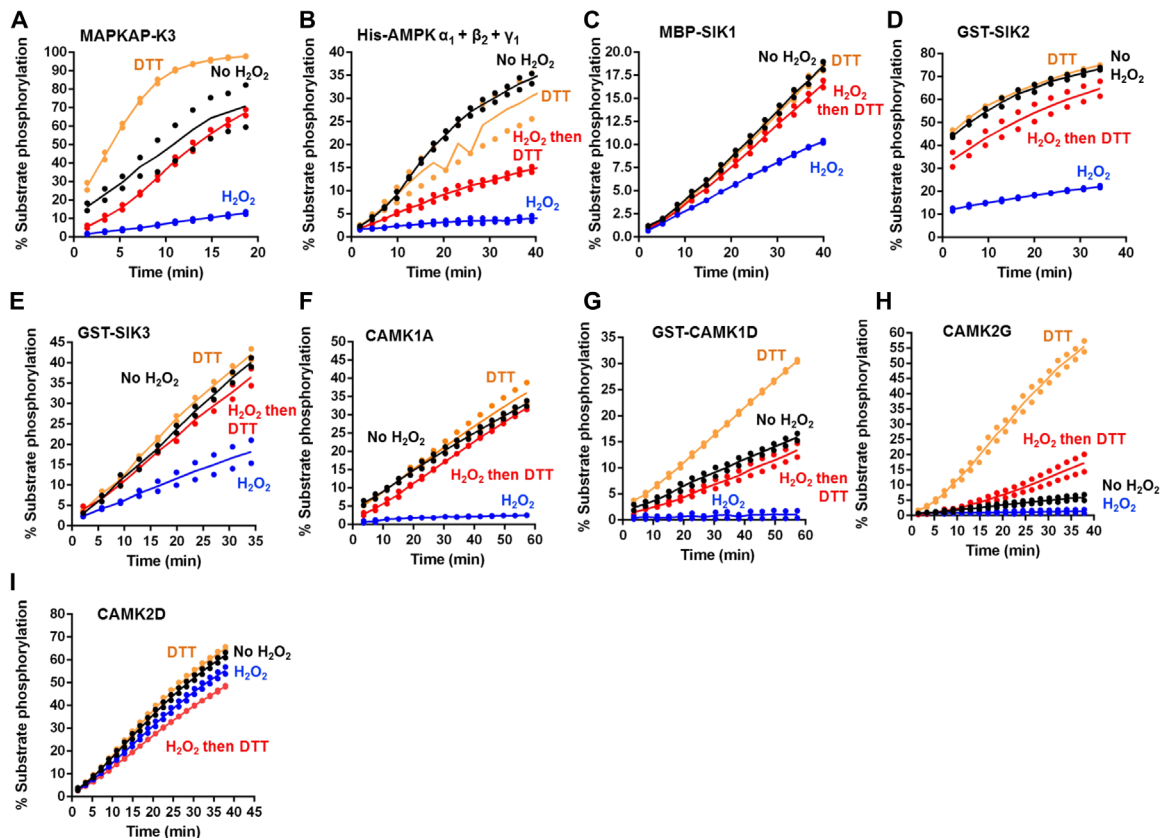


Fig. 9. Reversible oxidation of a conserved Cys residue regulates the activity of multiple Ser/Thr kinases. (A to I) A panel of AGC and CAMK-related kinases was probed for reversible oxidation-dependent inhibition using real-time phosphorylation of kinase-specific peptide substrates (table S3). In all assays, kinases were incubated on ice for 30 min in the presence or absence of 5 mM H_2O_2 . Reactions were then initiated with the addition 1 mM ATP and substrate peptide in the presence (where indicated) of 10 mM DTT. Kinases were assayed at the following final concentrations: (A) 15 nM MAPKAP-K3, (B) 24 ng of His-AMPK $\alpha_1 + \beta_2 + \gamma_1$, (C) 0.5 μM MBP-SIK1, (D) 2 nM GST-SIK2, (E) 2 nM GST-SIK3, (F) 0.7 μM CaMK1A, (G) 60 nM GST-CaMK1D, (H) 0.6 μM CaMK2G, or (I) 0.6 μM CaMK2D. In (F) to (I), CaMKs were supplemented with 5 mM CaCl_2 and 2 μM calmodulin. Kinetic data from $N = 2$ experiments performed in duplicate are shown.

involving cysteine (Cys^{290}), which is located in the conserved activation loop, C-terminal to the regulatory site of Thr^{288} autophosphorylation. Our new findings suggest that Cys oxidation and reduction can act dominantly over T-loop phosphorylation, providing an additional phosphorylation-independent layer of control over enzyme activity that might be important in eukaryotic cells. The specific nature of the oxidation event(s) in Aurora A is currently unclear but has recently been confirmed independently (98, 104), and we are undertaking detailed mass spectrometric investigations to distinguish between thiol species (11) present in Aurora A and other redox-sensitive kinases identified in this paper. The confirmation of sulfenylated Cys in Aurora A (Fig. 2) was of interest, because this is a reversible Cys modification and might therefore function as a bona fide signaling mechanism in response to cellular oxidative stress. Our recent work also established that Aurora A can be covalently modified by the sulfhydryl moiety of the Cys-containing metabolite coenzyme A under appropriate redox conditions and that an intermolecular disulfide bond with Cys^{290} in an adjacent Aurora A might contribute to an oxidative inhibitory mechanism (104). The location of the Cys^{290} residue on the activation loop (or T-loop) of Aurora A is notable, because this region is a well-known regulatory locus of catalytic activity in many ePKs (105, 106). We propose that Cys^{290} in

Aurora A is strategically positioned to be a dominant coordinator of redox regulation in response to ROS. This hypothesis has previously been explored for equivalent activation loop Cys residues including Cys^{200} of PKA (33, 57), Cys^{309} of AKT (107), Cys^{174} of AMPK (34), and Cys^{179} of CAMK1 (101).

Aurora A activity is modulated by reversible oxidation

The findings from our biochemical studies are supported by cellular data. We observed inhibition of TACC3 Ser^{558} phosphorylation (a physiological marker of Aurora A activity) in cells exposed to both oxidants and inducers of oxidation (Fig. 4). In addition, inhibition of Aurora A by H_2O_2 could be blocked by including ROS scavengers such as NAC and GSH in the medium, either restoring oxidized Aurora A back to a reduced, catalytically active state or by protection of Aurora A from irreversible overoxidation (Fig. 4). Phosphorylation of exogenous TACC3 could be induced through transient coexpression with a “redox-resistant” C290A Aurora A mutant, supporting a physiological regulatory role for the T-loop +2 Cys residue in the cellular context. Oxidative stress has been shown to impede mitotic progression of cells via a number of different mechanisms (108, 109). Previous observations demonstrated hyperphosphorylation of Aurora A at Thr^{288} in HeLa cells under oxidative stress (104, 110),

which might be a consequence of ROS-induced mitotic arrest. To ensure that changes in signaling were a direct consequence of oxidative modification of Aurora A and not just due to cell cycle inactivation (or activation) of the kinase, all of our experiments were performed using synchronized cells arrested in mitosis with nocodazole (5). However, given its complex spatiotemporal regulation, some caution should be applied when interpreting changes in Aurora A catalytic output, especially when changes in the cellular redox environment are suspected.

Evolutionary bioinformatics reveals that Cys is widespread in ePKs

The redox regulation of signaling enzymes is a rapidly expanding field of research enquiry. Whereas the majority of early research focused on the indirect targeting of kinases through oxidative inhibition of protein tyrosine phosphatases (111), there is now a wealth of evidence detailing direct oxidation of Cys and Met residues in protein kinases, where diversity within kinase groups and subfamilies has been reported (30, 112). However, although Cys-dependent redox regulation has been described within stress-activated protein kinase modules, including thioredoxin-regulated ASK1 (32, 113, 114), MEKK1 (29), MKK6 (115), and glutathione-responsive JNK and p38 α -MAPK (116), to our knowledge, no conserved mechanism has been described. However, none of these redox-regulated human MAPK, MAPKK, and MAPKKKs contain this conserved activation segment Cys residue (table S2) in contrast to the p38-MAPK targets MAPKAP-K2 and MAPKAP-K3, which we demonstrate here are rapidly inactivated by oxidation (Fig. 8).

Our comparative evolutionary analysis of protein kinomes revealed that ~11.5% of all protein kinases contain an analogous Cys residue to Cys²⁹⁰ in Aurora A (equivalent to Cys²⁰⁰ in PKA) at the “T-loop +2 position” in the activation segment (Fig. 5). However, only specific members of the AGC and CAMK subfamilies were enriched for this conserved Cys residue, and familiar kinases in these families including G protein-coupled kinases, PDK1, nuclear Dbf2-related (NDR)/large tumor suppressor (LATS) kinases, myosin light chain kinases, or death-associated protein kinases (DAPKs) do not have an evolutionary-conserved Cys at the Cys²⁹⁰ equivalent of Aurora A. Of 17 “T-loop +2 Cys”-containing kinases investigated, 14 were susceptible to reversible oxidative modulation. These included kinases for which redox sensitivity had previously been described, including AKT, AMPK, MELK, and CAMK1, as well as new potential targets for oxidative regulation, including SIK1 to SIK3, PLK1, PLK4, and MAPKAP-K2/3. We were also able to directly attribute redox inhibition in the T-loop +2 Cys residue in MAPKAP-K2 and PLK1 through comparative analysis of WT and Cys-Ala mutant proteins purified from human cells (Fig. 7). Some kinases that predicted to be redox-sensitive on the basis of the presence of an appropriate Cys residue in the activation segment, such as PKG and PhK, were resistant to peroxide inhibition, under identical experimental redox conditions that led to reversible modulation of related kinases. However, these (and other) kinases may still be sensitive to oxidation in cells, where peroxiredoxins have been shown to act as peroxide signal relays for kinases (117) and other proteins (118). A lack of appropriate chemical reactivity in an activation segment Cys might also help explain this observation, as observed for glyceraldehyde-3-phosphate dehydrogenase (119), and these data also prove that the concentrations of redox reagents in our standard assay do not induce effects through a nonspecific mechanism, such as protein de-

naturation. The intrinsic pK_a value (where K_a is the acid dissociation constant) of individual Cys residues, as well as their susceptibility to oxidation, is likely to be influenced by networks of interacting amino acids, phosphorylated amino acids, solvent accessibility, protein-protein interactions, and structural dynamics (64, 98, 120). In this context, artificial incorporation of a Cys residue at the equivalent position in EPHA3 did not sensitize this Tyr kinase to oxidation (fig. S12), suggesting that the EPHA3 activation loop is potentially in an unfavorable environment to stabilize reactive Cys residues. Moreover, the relative reactivity of a Cys residue is likely to be context-specific and could vary between different allosteric activation states. In this regard, note that Cys²⁹⁰ transitions from being exposed, to buried, in TPX2-bound Aurora A (104), although it is not immediately obvious to what extent this reconfiguration translates to a reversible change in Cys reactivity.

The presence of a Cys-containing activation segment is a conserved feature of most eukaryotic CAMK and AGC family kinases

Closer inspection of the activation segment confirms that although Cys is present at all possible positions in the activation segment across various kinomes (fig. S8F), two sites, DFG +2 (5.1%) and T-loop +2 (11.5%), dominate evolutionary Cys conservation in this region. Both Cys residues acids are coconserved in ~1.4% of all ePKs in our database (Fig. 5A, bottom), where, in the context of redox regulation, they are believed to support intramolecular and/or intermolecular autoinhibitory disulfide bonds in AKT and MELK (and perhaps p21-activated protein kinases, p70S6k, and PKC isozymes; table S2 and fig. S13). Consistent with this prediction, the introduction of a Cys residue at the DFG +2 position in Aurora A changed both thermal stability and redox regulation so that it behaved much more like AKT and MELK. Moreover, we obtained MS data that confirmed the formation of an intramolecular disulfide bond between Cys²⁹⁰ and an artificially engineered Cys²⁷⁸ (Fig. 7G), which likely explains the acquired obligate dependency on reducing agents to activate S278C Aurora A.

Further structural and proteomics efforts are required to decipher the molecular processes involved in oxidative regulation of Ser/Thr protein kinases and to assess the relative contribution of different reversible Cys oxidized states (e.g., sulfenic acids, sulfenyl-amides, and intra- and intermolecular disulfide bonds) in modulating signaling.

Our study opens new avenues to explore functional relationships between physiological ROS-based signaling networks and the broader redox-regulated kinome, especially mechanisms that occur through conserved activation segment Cys residues. Mitochondrial damage and the associated elevation of ROS are implicated in a range of human diseases including aging (121), cancer (122), and neural degenerative disorders such as Parkinson's disease (123) and a multitude of factors, including hypoxia, contribute to sustained high ROS levels in tumors (124). A key line of enquiry, therefore, will be to explore the impact of chronic oxidative stress and increased sulfenylated protein populations on both normal and pathological Ser/Thr kinase functions. The extent to which oxidation of kinases may influence the therapeutic efficacy of inhibitor compounds in a cellular context is also of interest, especially for kinases targeted by Cys-based covalent mechanisms. Aurora A inhibitors target distinct conformational species, which can be broadly separated into compounds with preferences for the DFG-in or DFG-out states (72, 125, 126).

The ability of oxidative modifications in the activation segment to alter this “DFG equilibrium” may also have implications for the selectivity of inhibitors in cells, where the propensity of redox-active Cys residues in Ser/Thr kinases to undergo sulfenylation could be exploited for the rationale design of new classes of covalent inhibitors. This strategy has been adapted to great success to generate clinical compounds with potency and selectivity toward tyrosine kinases, such as afatinib and osimertinib, which target Cys⁷⁹⁷ of the redox-regulated tyrosine kinase EGFR for the treatment of non-small cell lung cancer (127). Last, a deeper mechanistic understanding of the dynamics of Ser/Thr kinase redox regulation may reveal Cys residues that are differentially exposed in active and inactive kinase conformations and potentially lead to a versatile reservoir of new covalent drug targets.

MATERIALS AND METHODS

Recombinant proteins and general reagents

Commercial recombinant protein kinase fusion proteins were purchased from Medical Research Council Protein Phosphorylation and Ubiquitylation Unit (PPUU) reagents (University of Dundee) and were purified from Sf21 cells or *E. coli*. Full details are provided in table S3. GST and His6-tagged kinases were purified using standard procedures, before storage in 1 mM DTT (except where indicated) at -80°C . All kinases were assayed using standard enzyme preparations (128). Bacterially expressed GST-MAPKAP-K2 and GST-MAPKAP-K3 were activated *in vitro* by incubation with catalytically active p38 α , which was removed by repurification before assay. General biochemicals and all redox reagents, including GRX, were purchased from Sigma-Aldrich.

Protein kinase assays

Kinase assays were performed using nonradioactive real-time mobility shift-based microfluidic assays, as described previously (66, 91, 129, 130), in the presence of 2 μM of the appropriate fluorescent-tagged peptide substrate (table S2) and 1 mM ATP (unless specified otherwise). Pressure and voltage settings were adjusted manually to afford optimal separation of phosphorylated and nonphosphorylated peptides. All assays were performed in 50 mM Hepes (pH 7.4), 0.015% (v/v) Brij-35, and 5 mM MgCl₂, and the real-time or end point degree of peptide phosphorylation was calculated by differentiating the ratio of the phosphopeptide:peptide present in the reaction. Kinase activity in the presence of different redox reagents was quantified by monitoring the generation of phosphopeptide during the assay, relative to controls. Data were normalized with respect to control assays, with phosphate incorporation into the peptide generally limited to <20% to prevent depletion of ATP and to ensure assay linearity. ATP K_M and the concentration of a compound that caused IC₅₀ values were determined by nonlinear regression analysis using GraphPad Prism software. Where specified, kinase assays using Aurora A were supplemented with 100 nM GST-TPX2 or GST alone. Assays for CAMK kinases included 5 mM CaCl₂ and 2 μM calmodulin as standard. Where appropriate, PKG1 assays were performed in the presence of 1 mM cGMP. Recovery of Aurora A activity from oxidative inhibition was assessed by monitoring substrate phosphorylation in the presence of peroxide in real time, followed by subsequent introduction of DTT or GSH. To standardize this real-time reversible redox regulation assay for all kinases, enzymes were preincubated in the presence or absence of 5 mM H₂O₂ on ice for 30 min, and

then substrate phosphorylation was initiated with the addition of 1 mM ATP and the appropriate substrate peptide in the presence (where indicated) of 10 mM DTT unless otherwise stated. Aurora A kinase assays were also developed with recombinant GST-TACC3 as a substrate. Kinase assays were initiated after the addition of GST-TACC3 (1 μg) in the presence of 0.5 mM ATP and 5 mM MgCl₂ and TACC3 Ser⁵⁵⁸ phosphorylation were detected by immunoblotting with a pSer⁵⁵⁸ TACC3 antibody after 15-min assay time, as previously described (74). Reactions were terminated by the addition of SDS loading buffer. Equal loading of TACC3 substrate and Aurora A was confirmed with an anti-TACC3 antibody and antibodies for total and phosphorylated Aurora A (pThr²⁸⁸). Aurora A autophosphorylation after phosphatase treatment was also detected using a previously described Thr²⁸⁸ phospho-specific antibody (74). Dephosphorylated Aurora A (1 μg) was produced by coexpression with λPP in *E. coli* and then incubated with 1 mM ATP and 10 mM MgCl₂ for the indicated time periods under reducing (+1 mM DTT) or oxidizing (+1 mM H₂O₂) conditions in the presence and absence of 1 μg of GST-TPX2, 1 μg of GST, or 100 μM MLN8237. Reactions were terminated by the addition of SDS gel-loading buffer.

Cloning and recombinant protein purification from *E. coli*

For enzyme and DSF assays, murine or human Aurora A, MELK (1 to 340), PLK1 (1 to 364), PLK4 (1 to 369), full-length PKA, EPHA3 (kinase domain and juxtamembrane region), ABL (46 to 515), TACC3, and TPX2 (1 to 43) were produced in BL21 (DE3) pLysE *E. coli* cells (Novagen) with expression induced with 0.5 mM isopropyl- β -D-thiogalactopyranoside for 18 hours at 18°C and purified as N-terminal His6-tag or N-terminal His6-GST tag fusion proteins by affinity chromatography and size exclusion chromatography using a HiLoad 16/600 Superdex 200 column (GE Healthcare) equilibrated in 50 mM tris-HCl (pH 7.4), 100 mM NaCl, and 10% (v/v) glycerol. Where appropriate, recombinant protein was purified in the presence of 1 mM DTT. Ser²⁷⁸Ala, Ser²⁷⁸Cys, Cys²⁹⁰Ala Aurora A, and equivalent Cys-Ala mutants of other kinases were generated using standard mutagenic procedures and purified as described above (66). To generate a phosphorylation-depleted kinase, Aurora A was coexpressed with λPP in BL21 (DE3) pLysE *E. coli* cells before purification; λPP was subsequently removed by immobilized metal affinity chromatography and size exclusion chromatography.

Differential scanning fluorimetry

Thermal shift assays were performed with a StepOnePlus real-time polymerase chain reaction (PCR) machine (Life Technologies) using SYPRO Orange dye (Invitrogen) and thermal ramping (0.3°C in step intervals between 25° and 94°C). All proteins were diluted to a final concentration of 5 μM in 50 mM tris-HCl (pH 7.4) and 100 mM NaCl in the presence or absence of the indicated concentrations of ATP, H₂O₂, DTT, GSH, or MLN8237 [final dimethyl sulfoxide (DMSO) concentration no higher than 4% (v/v)] (131) and were assayed as described previously (67). Normalized data were processed using the Boltzmann equation to generate sigmoidal denaturation curves, and average $T_m/\Delta T_m$ values were calculated as previously described (132) using GraphPad Prism software.

Human cell culture and cell treatments

HeLa cells were cultured in Dulbecco's modified Eagle medium (Lonza) supplemented with 10% fetal bovine serum (HyClone),

penicillin (50 U/ml), and streptomycin (0.25 µg/ml) (Lonza) and maintained at 37°C in 5% CO₂ humidified atmosphere. To examine the effects of oxidative stress on Aurora A kinase activity, cells were arrested in mitosis with 100 nM nocodazole for 16 hours and then treated with a range of concentrations of H₂O₂, menadione, or diamide for 30 to 60 min. To stimulate chronic oxidative stress, arrested HeLa cells were collected and washed in phosphate-buffered saline (PBS), and fresh culture medium containing GO at a nontoxic concentration (2 U/ml) and 100 nM nocodazole was added. Subsequently, cells were collected and harvested periodically over a 2-hour time period. To investigate reversible inactivation of Aurora A by peroxide, arrested cells were incubated for 10 min with 10 mM H₂O₂, and then peroxide-containing medium was removed and replaced with fresh culture medium containing 10 mM DTT, NAC or GSH, or buffer control. To examine TACC3 phosphorylation by exogenous Aurora A, HeLa cells were transiently transfected with pcDNA3 encoding full-length WT or C290A N-terminal Myc-tagged Aurora A and pBrain-GFP-TACC3KDP-shTACC3 (to simultaneously express N-terminal tagged GFP-TACC3 and suppress the expression of endogenous TACC3; Addgene), using Lipofectamine 3000 (Thermo Fisher Scientific). Three micrograms of DNA (for each plasmid) was used to transfect six-well plate dishes of HeLa cells, and the medium was changed after 3 hours. Equal volumes of transfection reagent were used for both single and cotransfections. Transfected HeLa cells were synchronized with nocodazole as previously described 24 hours after transfection and then treated with various concentrations of diamide for 30 min. In all assays, cells were subsequently washed in PBS, harvested in bromophenol blue-free SDS sample buffer supplemented with 1% Triton X-100, protease inhibitor cocktail tablet, and a phosphatase inhibitor tablet (Roche), and sonicated briefly before immunoblotting.

Human cell lysis, immunoprecipitation, and Western blot analysis

Total cell lysates were centrifuged at 20,817g for 20 min at 4°C, and the supernatant was preserved for further analysis. Samples were initially diluted 50-fold, and protein concentration was measured using the Coomassie Plus Staining Reagent (Bradford) Assay Kit (Thermo Fisher Scientific) and processed for immunoblotting with TACC3 or Aurora A antibodies as described (74, 90). To assay the kinase activity of T-loop +2 Cys-containing kinases immunoprecipitated from human cells, WT and Cys-Ala full-length variants of MAPKAP-K2 and PLK1 (C244A and C212A, respectively) were cloned into a pcDNA3 vector and expressed with a 3C protease cleavable, N-terminal Myc tag. All immunoprecipitation experiments used HEK 293T cells transfected using a 3:1 polyethylenimine [average *M_w* (weight-average molecular weight), ~25,000 Da; Sigma-Aldrich] to DNA ratio (60:20 µg, for a single 10-cm culture dish). Cells were treated with 4 mM valproic acid 24 hours after transfection, and proteins were harvested the following day using a lysis buffer containing 50 mM tris-HCl (pH 7.4), 150 mM NaCl, 0.1% (v/v) Triton X-100, and 5% (v/v) glycerol and supplemented with a protease inhibitor cocktail tablet and a phosphatase inhibitor tablet (Roche). Lysates were briefly sonicated on ice and clarified by centrifugation at 20,817g for 20 min at 4°C, and the resulting supernatants were incubated with Pierce Anti-c-Myc-Agarose resin (Thermo Fisher Scientific) for 1 hour with gentle end over end mixing at 4°C. Agarose beads containing bound protein were collected and washed three times in 50 mM tris-HCl (pH 7.4) and

500 mM NaCl and then equilibrated in storage buffer [50 mM tris-HCl (pH 7.4), 100 mM NaCl, and 5% (v/v) glycerol]. The purified kinases were then proteolytically eluted from the beads over a 3-hour period using 3C protease (0.5 µg) at 4°C with gentle agitation and then assayed using real-time microfluidic peptide assay as described above.

Detection of sulfenylated and glutathionylated proteins by immunoblotting

Recombinant Aurora A (0.5 µg) was incubated with 50 mM tris-HCl (pH 7.4) and 100 mM NaCl in the presence of different concentrations of H₂O₂ or 10 mM DTT for 10 min. Cysteine sulfenic acid was detected by SDS-polyacrylamide gel electrophoresis (PAGE) and immunoblotting after adduct formation with 1 mM dimedone for 20 min. Dimedone stocks were prepared in DMSO with a final assay DMSO concentration no higher than 4% (v/v). To detect glutathionylation of proteins, 1 µg of proteins was incubated with 10 mM GSSG or GSH for 30 min, and glutathione-protein complexes were detected by immunoblotting after nonreducing SDS-PAGE. Comparative changes in the electrophoretic mobility of Aurora A in the presence of DTT and H₂O₂ were also detected with antibodies for total and pThr²⁸⁸ Aurora A, and SDS-PAGE was performed under reducing and nonreducing conditions. All incubations were performed at 20°C.

Aurora A sample preparation for MS analysis of intramolecular disulfide bond formation

Five micrograms of Aurora A purified in the absence of DTT was heated at 80°C in 0.06% (w/v) RapiGest SF (Waters) dissolved in 25 mM ammonium bicarbonate for 10 min. Samples were digested overnight at 25°C using a 20:1 (w/w) ratio of Aurora A:Chymotrypsin (Promega), with shaking at 600 rpm. The sample was equally split into two, one aliquot of which was reduced with DTT (3 mM) at 60°C for 10 min, cooled, and alkylated with 10 mM iodoacetamide (IAA) at room temperature for 30 min in the dark. Excess IAA was quenched by addition of DTT to a final concentration of 7 mM. The second sample was left on ice. RapiGest hydrolysis was induced in both samples by the addition of 1.5% (v/v) trifluoroacetic acid (TFA) and 3% (v/v) acetonitrile, shaking at 600 rpm and 37°C for 2 hours. Insoluble products were removed by centrifugation (13,000g for 15 min at 4°C). Samples were subjected to strong cation exchange using in-house packed stage tips (Empore Supelco 47-mm Cation Exchange disk #2251), three disks per 200 µl of tip. All centrifugation steps were performed at 2000g for 3 min until all liquid had passed through the stage tip. Briefly, tips were equilibrated with sequential washes in acetone, methanol, water, 5% (v/v) ammonium hydroxide, and water (2 × 200 µl of each). Peptide samples were thrice passed through the equilibrated stage tip and washed with 250 µl of 1.5% (v/v) TFA, before elution with 250 µl of 5% (v/v) ammonium hydroxide. Eluted material was dried using cooled vacuum centrifugation. Peptides were solubilized in 20 µl of 3% (v/v) acetonitrile and 0.1% (v/v) TFA and sonicated for 10 min before centrifugation (13,000g for 15 min at 4°C) to remove insoluble material before LC-MS/MS analysis.

Liquid chromatography mass spectrometry (LC-MS) analysis of WT and S278C Aurora A

Peptides were separated on a Ultimate 3000 nano system (Dionex) by reverse-phase high-performance liquid chromatography, using a

trapping column (PepMap 100, C18, 300 μm by 5 mm) equilibrated in loading buffer [3% (v/v) acetonitrile and 0.1% (v/v) TFA] at a flow rate of 9 $\mu\text{l}/\text{min}$ for 7 min. Chromatographic separation was performed using an EASY-Spray C18 column (75 μm by 500 mm, 2- μm bead diameter) at a flow rate of 0.3 $\mu\text{l}/\text{min}$ over a 30-min gradient from 3% buffer A [0.1% (v/v) formic acid]:97% buffer B [80% (v/v) acetonitrile and 0.1% (v/v) formic acid] to 20% buffer A:80% buffer B. Data were acquired using a Thermo Orbitrap Fusion Lumos Tribrid mass spectrometer (Thermo Fisher Scientific). All spectra were acquired in the Orbitrap in a data-dependent analysis mode using a top speed approach (3-s cycle time), with ions being subjected to higher-energy collisional dissociation (HCD) (normalized collision energy of 32%). MS1 parameters: 60K resolution at 200 mass/charge ratio (m/z); AGC, 4×10^5 ; maximum injection time, 50 ms; mass range, 350 to 2000; charge stated, 2+ to 6+. MS2 parameters: 30K resolution at 200 m/z ; AGC, 5×10^4 ; maximum injection time, 54 ms. A dynamic exclusion window was applied for 60 s at a tolerance of 10 parts per million (ppm).

MS data analysis

pLink-SS software was used to initially identify spectra containing disulfide-linked peptides, as previously described (133). Precursor and fragment tolerances were set to 10 ppm, variable modifications of Cys carbamidomethylation, and Ser/Thr phosphorylation. Once a spectrum containing a disulfide-linked peptide was identified, the spectrum was redrawn using a custom R script and manually annotated to include disulfide fragmentation mass shifts of -33.987 atomic mass units (amu) (dehydroalanine) and $+31.971$ amu (disulfohydril) at both Cys residues (134).

Identification, alignment, and visualization of protein kinase-related sequences

The Multiply-Aligned Profiles for Global Alignment of Protein Sequences (MAPGAPS) procedure (135) was used alongside a variety of curated ePKs profiles (129, 136–138) to identify and align ePK-related sequences from the nonredundant sequence database and UniProt reference proteome (139) databases (Release 2018_09). Sequences with a Cys residue at the Aurora A Cys²⁹⁰-equivalent position were retrieved and used for further taxonomic analysis. Taxonomic information was based on National Center for Biotechnology Information Taxonomy database (140) and WebLogos (141) were generated using WebLogo version 2.8. Amino acids were colored on the basis of their chemical properties. Polar (G, S, T, Y, C, Q, and N), basic (K, R, and H), acidic (D and E), and hydrophobic (A, V, L, I, P, W, and M) amino acids are colored green, blue, red, and black, respectively.

Yeast strains, plasmids, and growth conditions

S. pombe cells (table S4) were transformed with the indicated plasmids and grown at 30°C in synthetic minimal medium (Edinburgh minimal medium 2) supplemented with histidine (100 mg/liter), adenine (87 to 100 mg/liter), uracil (75 mg/liter) and, where indicated, thiamine (20 $\mu\text{g}/\text{ml}$) (142). The WT *srk1* gene (including intron) was amplified from *S. pombe* genomic DNA by PCR, and *srk*^{C324A} and *srk1*^{C324S} were generated synthetically, PCR-amplified, and ligated into Nde I and Bam HI sites in pRep41HM (143) to generate pRep41HMsrk1, pRep41HMsrk^{C324A}, and pRep41HMsrk^{C324S} expressing His Myc-tagged Srk1, Srk1^{C324A}, or Srk1^{C324S} from the nmt41 promoter. WT *pka1* open reading frame, without the stop

codon, was amplified from *S. pombe* genomic DNA and cloned into pJet1.2. *pka1*^{C358S} was amplified from genomic DNA by a two-step overlapping PCR to introduce the mutation. Pka1^{C358A} was generated synthetically. WT and *pka1* mutant genes were then subcloned into Nde I and Bam HI sites in pRep41pkC (143) to generate pRep41Pka1pkc, pRep41Pka1^{C358S}pkc, and pRep41Pka1^{C358A}pkc expressing C-terminally protein kinase-tagged Pka1, Pka1^{C358S}, or Pka1^{C358A} from the nmt41 promoter. All primer sequences are available upon request.

Analysis of *S. pombe* proteins by immunoblotting

Equal amounts of exponentially growing cells (9×10^6 to 1×10^7 cells) were added to 20% trichloroacetic acid, harvested by centrifugation at 3000 rpm for 1 min, and then snap-frozen in liquid nitrogen. Protein was extracted as described previously (144) but without phosphatase treatment. Proteins were resuspended in 1% SDS, 1 mM EDTA, and 100 mM tris-HCl (pH 8.0) containing 10 mM *N*-ethylmaleimide. Protein concentrations were estimated using the bicinchoninic acid protein assay (Thermo Fisher Scientific), and equal amounts of protein (5 to 10 μg) were resolved on 8% SDS-PAGE gels, followed by transfer to nitrocellulose membrane and analysis by immunoblotting as previously described (145) using the following antibodies: anti-myc (9E10, Santa Cruz Biotechnology), anti-tubulin (anti-Tat1), phospho-PKA substrate antibody (RRXS*/T*, 100G7E, Cell Signaling Technology), and anti-Pka (V5 epitope monoclonal antibody, V8012, Sigma-Aldrich). Images were collected using enhanced chemiluminescence reagent (Pierce ECL Plus, Thermo Fisher Scientific) and ImageQuant software (Typhoon FLA9500) or VILBER Fx6 / Fx7 Chemiluminescent System (Labtech).

Analysis of *S. pombe* cell length at division and CDC25-GFP localization

Exponentially growing *S. pombe* were resuspended in PBS and mounted onto poly-L-lysine coated slides. Differential interference contrast images were taken using a Zeiss AxioScope, and cell lengths were compared by measuring >94 newly divided cells for each sample. For analysis of fluorescence (CDC25-GFP localization), cells were mounted in VECTASHIELD containing 4',6-diamidino-2-phenylindole (DAPI) (1.5 $\mu\text{g}/\text{ml}$) to visualize DNA and observed on a Zeiss AxioScope fluorescence microscope using appropriate filters.

Assessing growth and salt stress sensitivity of *S. pombe*

Equal numbers of exponentially growing WT(JX333) or $\Delta pka1$ (JX384) cells transformed with pRep41pkc(vector), pRep41Pka1pkc, pRep41Pka1^{C358S}pkc, or pRep41Pka1^{C358A}pkc grown in Edinburgh minimal medium (EMM) supplemented with adenine (100 mg/liter) and thiamine (20 $\mu\text{g}/\text{ml}$) (EMMAT) were serially diluted (10-fold dilutions then spotted onto an EMMAT agar plate or EMMAT agar plates containing 1 M KCl). Plates were incubated at 30°C for 2 to 5 days and imaged at 24-hour intervals until comparable levels of growth were observed for the WT cells on each plate.

Statistical analysis

All experimental procedures were repeated in at least three separate experiments with matched positive and negative controls (unless stated otherwise). Results are expressed as means \pm SD for all in vitro experiments, and data are expressed as the means \pm SD. When applied, statistical significance of differences ($*P \leq 0.05$) was assessed using

a Student's *t* test for normally distributed data. All statistical tests were performed using Prism 7 (GraphPad Software).

SUPPLEMENTARY MATERIALS

stke.sciencemag.org/cgi/content/full/13/639/eaax2713/DC1

Fig. S1. Chemical routes for Cys redox modifications in proteins and their detection with commercial reagents.

Fig. S2. Analysis of Aurora A purified in the presence of DTT.

Fig. S3. Biochemical analysis of Aurora A oxidation.

Fig. S4. Analysis of Aurora A and a redox-resistant C290A mutant.

Fig. S5. Analysis of C290S and C290D mutants.

Fig. S6. Both WT and C290A Aurora A bind to TPX2.

Fig. S7. Reversible glutathionylation of Aurora A and AKT.

Fig. S8. Taxonomic analysis of conserved Cys residues within the activation segment of all ePKs.

Fig. S9. Biochemical analysis of Cys-containing protein kinases.

Fig. S10. Thermal profiling and immunoblotting-based redox analysis of Aurora A "DFG +2" kinase mutants.

Fig. S11. Kinases having a "T-loop +2" Cys residue that are insensitive to redox-dependent regulation.

Fig. S12. Real-time redox analysis of model Tyr kinases and Cys mutants.

Fig. S13. Structural models of disulfide-based mechanisms involving activation segment Cys in Ser/Thr kinases.

Table S1. Human kinases containing an Aurora A Cys²⁹⁰ equivalent in the activation segment.

Table S2. Positional distribution in all human kinases that contain Cys residues in the activation segment.

Table S3. Protein kinase enzymes and substrates.

Table S4. Yeast strains described in this study.

References (146, 147)

[View/request a protocol for this paper from Bio-protocol.](#)

REFERENCES AND NOTES

- T. Finkel, Signal transduction by reactive oxygen species. *J. Cell Biol.* **194**, 7–15 (2011).
- B. C. Dickinson, C. J. Chang, Chemistry and biology of reactive oxygen species in signaling or stress responses. *Nat. Chem. Biol.* **7**, 504–511 (2011).
- J. B. Behring, S. van der Post, A. D. Mooradian, M. J. Egan, M. I. Zimmerman, J. L. Clements, G. R. Bowman, J. M. Held, Spatial and temporal alterations in protein structure by EGF regulate cryptic cysteine oxidation. *Sci. Signal.* **13**, eaay7315 (2020).
- C. E. Paulsen, K. S. Carroll, Orchestrating redox signaling networks through regulatory cysteine switches. *ACS Chem. Biol.* **5**, 47–62 (2010).
- J. C. Patterson, B. A. Joughin, B. van de Kooij, D. C. Lim, D. A. Lauffenburger, M. B. Yaffe, ROS and oxidative stress are elevated in mitosis during asynchronous cell cycle progression and are exacerbated by mitotic arrest. *Cell Syst.* **8**, 163–167.e2 (2019).
- Y. H. Seo, K. S. Carroll, Profiling protein thiol oxidation in tumor cells using sulfenic acid-specific antibodies. *Proc. Natl. Acad. Sci. U.S.A.* **106**, 16163–16168 (2009).
- S. G. Rhee, S. W. Kang, W. Jeong, T.-S. Chang, K.-S. Yang, H. A. Woo, Intracellular messenger function of hydrogen peroxide and its regulation by peroxiredoxins. *Curr. Opin. Cell Biol.* **17**, 183–189 (2005).
- V. Gupta, K. S. Carroll, Sulfenic acid chemistry, detection and cellular lifetime. *Biochim. Biophys. Acta* **1840**, 847–875 (2014).
- A. Salmeen, J. N. Andersen, M. P. Myers, T.-C. Meng, J. A. Hinks, N. K. Tonks, D. Barford, Redox regulation of protein tyrosine phosphatase 1B involves a sulphenyl-amide intermediate. *Nature* **423**, 769–773 (2003).
- R. L. M. van Montfort, M. Congreve, D. Tisi, R. Carr, H. Jhoti, Oxidation state of the active-site cysteine in protein tyrosine phosphatase 1B. *Nature* **423**, 773–777 (2003).
- H. J. Forman, M. J. Davies, A. C. Krämer, G. Miotto, M. Zaccarin, H. Zhang, F. Ursini, Protein cysteine oxidation in redox signaling: Caveats on sulfenic acid detection and quantification. *Arch. Biochem. Biophys.* **617**, 26–37 (2017).
- C. L. Grek, J. Zhang, Y. Manevich, D. M. Townsend, K. D. Tew, Causes and consequences of cysteine S-glutathionylation. *J. Biol. Chem.* **288**, 26497–26504 (2013).
- A. N. Anselmo, M. H. Cobb, Protein kinase function and glutathionylation. *Biochem. J.* **381**, e1–e2 (2004).
- F. Q. Schafer, G. R. Buettner, Redox environment of the cell as viewed through the redox state of the glutathione disulfide/glutathione couple. *Free Radic. Biol. Med.* **30**, 1191–1212 (2001).
- J. B. Owen, D. A. Butterfield, Measurement of oxidized/reduced glutathione ratio, in *Protein Misfolding and Cellular Stress in Disease and Aging* (Springer, 2010), pp. 269–277.
- P. Maher, The effects of stress and aging on glutathione metabolism. *Ageing Res. Rev.* **4**, 288–314 (2005).
- I. Dalle-Donne, R. Rossi, D. Giustarini, R. Colombo, A. Milzani, S-glutathionylation in protein redox regulation. *Free Radic. Biol. Med.* **43**, 883–898 (2007).
- G. Manning, G. D. Plowman, T. Hunter, S. Sudarsanam, Evolution of protein kinase signaling from yeast to man. *Trends Biochem. Sci.* **27**, 514–520 (2002).
- B. Nolen, S. Taylor, G. Ghosh, Regulation of protein kinases; controlling activity through activation segment conformation. *Mol. Cell* **15**, 661–675 (2004).
- L. N. Johnson, M. E. Noble, D. J. Owen, Active and inactive protein kinases: Structural basis for regulation. *Cell* **85**, 149–158 (1996).
- N. Kannan, A. F. Neuwald, Did protein kinase regulatory mechanisms evolve through elaboration of a simple structural component? *J. Mol. Biol.* **351**, 956–972 (2005).
- N. K. Tonks, Redox redux: Revisiting PTPs and the control of cell signaling. *Cell* **121**, 667–670 (2005).
- C. E. Paulsen, T. H. Truong, F. J. Garcia, A. Homann, V. Gupta, S. E. Leonard, K. S. Carroll, Peroxide-dependent sulfenylation of the EGFR catalytic site enhances kinase activity. *Nat. Chem. Biol.* **8**, 57–64 (2011).
- T. H. Truong, K. S. Carroll, Redox regulation of epidermal growth factor receptor signaling through cysteine oxidation. *Biochemistry* **51**, 9954–9965 (2012).
- D. E. Heppner, C. M. Dustin, C. Liao, M. Hristova, C. Veith, A. C. Little, B. A. Ahlers, S. L. White, B. Deng, Y.-W. Lam, J. Li, A. van der Vliet, Direct cysteine sulfenylation drives activation of the Src kinase. *Nat. Commun.* **9**, 4522 (2018).
- D. J. Kemble, G. Sun, Direct and specific inactivation of protein tyrosine kinases in the Src and FGFR families by reversible cysteine oxidation. *Proc. Natl. Acad. Sci. U.S.A.* **106**, 5070–5075 (2009).
- E. Giannoni, F. Buricchi, G. Raugei, G. Ramponi, P. Chiarugi, Intracellular reactive oxygen species activate Src tyrosine kinase during cell adhesion and anchorage-dependent cell growth. *Mol. Cell. Biol.* **25**, 6391–6403 (2005).
- F. Cuello, P. Eaton, Cysteine-based redox sensing and its role in signaling by cyclic nucleotide-dependent kinases in the cardiovascular system. *Annu. Rev. Physiol.* **81**, 63–87 (2018).
- J. V. Cross, D. J. Templeton, Oxidative stress inhibits MEK1 by site-specific glutathionylation in the ATP-binding domain. *Biochem. J.* **381**, 675–683 (2004).
- A. Corcoran, T. G. Cotter, Redox regulation of protein kinases. *FEBS J.* **280**, 1944–1965 (2013).
- J. R. Burgoyne, M. Madhani, F. Cuello, R. L. Charles, J. P. Brennan, E. Schröder, D. D. Browning, P. Eaton, Cysteine redox sensor in PKGα enables oxidant-induced activation. *Science* **317**, 1393–1397 (2007).
- P. J. Nadeau, S. J. Charette, J. Landry, REDOX reaction at ASK1-Cys250 is essential for activation of JNK and induction of apoptosis. *Mol. Biol. Cell* **20**, 3628–3637 (2009).
- K. M. Humphries, J. K. Pennypacker, S. S. Taylor, Redox regulation of cAMP-dependent protein kinase signaling: Kinase versus phosphatase inactivation. *J. Biol. Chem.* **282**, 22072–22079 (2007).
- D. Shao, S.-i. Oka, T. Liu, P. Zhai, T. Ago, S. Sciarretta, H. Li, J. Sadoshima, A redox-dependent mechanism for regulation of AMPK activation by Thioredoxin1 during energy starvation. *Cell Metab.* **19**, 232–245 (2014).
- L.-S. Cao, J. Wang, Y. Chen, H. Deng, Z.-X. Wang, J.-W. Wu, Structural basis for the regulation of maternal embryonic leucine zipper kinase. *PLOS ONE* **8**, e70031 (2013).
- H. Murata, Y. Ihara, H. Nakamura, J. Yodoi, K. Sumikawa, T. Kondo, Glutaredoxin exerts an antiapoptotic effect by regulating the redox state of Akt. *J. Biol. Chem.* **278**, 50226–50233 (2003).
- J. J. Sjölander, A. Tarczykowska, C. Picazo, I. Cossio, I. N. Redwan, C. Gao, C. Solano, M. B. Toledano, M. Grøtli, M. Molin, P. Sunnerhagen, A redox-sensitive thiol in Wis1 modulates the fission yeast MAPK response to H₂O₂ and is the target of a small molecule. *Mol. Cell. Biol.* **40**, e00346-19 (2020).
- H. Kalyanaram, S. Zhuang, R. B. Pilz, D. E. Casteel, The activity of cGMP-dependent protein kinase Ia is not directly regulated by oxidation-induced disulfide formation at cysteine 43. *J. Biol. Chem.* **292**, 8262–8268 (2017).
- J. R. Burgoyne, S.-i. Oka, N. Ale-Agha, P. Eaton, Hydrogen peroxide sensing and signaling by protein kinases in the cardiovascular system. *Antioxid. Redox Signal.* **18**, 1042–1052 (2013).
- J. L. Sheehee, A. D. Bonev, A. M. Schmoker, B. A. Ballif, M. T. Nelson, T. M. Moon, W. R. Dostmann, Oxidation of cysteine 117 stimulates constitutive activation of the type Ia cGMP-dependent protein kinase. *J. Biol. Chem.* **293**, 16791–16802 (2018).
- O. Prysyzhna, O. Rudyk, P. Eaton, Single atom substitution in mouse protein kinase G eliminates oxidant sensing to cause hypertension. *Nat. Med.* **18**, 286–290 (2012).
- S. Butterworth, D. A. E. Cross, M. R. V. Finlay, R. A. Ward, M. J. Waring, The structure-guided discovery of osimertinib: The first U.S. FDA approved mutant selective inhibitor of EGFR T790M. *MedChemComm* **8**, 820–822 (2017).
- Z. Zhao, Q. Liu, S. Bliven, L. Xie, P. E. Bourne, Determining cysteines available for covalent inhibition across the human kinome. *J. Med. Chem.* **60**, 2879–2889 (2017).

44. Q. Liu, Y. Sabnis, Z. Zhao, T. Zhang, S. J. Buhrlage, L. H. Jones, N. S. Gray, Developing irreversible inhibitors of the protein kinase cysteinome. *Chem. Biol.* **20**, 146–159 (2013).
45. D. P. Byrne, D. M. Foulkes, P. A. Eyers, Pseudokinases: Update on their functions and evaluation as new drug targets. *Future Med. Chem.* **9**, 245–265 (2017).
46. A. Chaikuad, P. Koch, S. A. Laufer, S. Knapp, The cysteinome of protein kinases as a target in drug development. *Angew. Chem. Int. Ed.* **57**, 4372–4385 (2018).
47. J. R. Bischoff, L. Anderson, Y. Zhu, K. Mossie, L. Ng, B. Souza, B. Schryver, P. Flanagan, F. Clairvoyant, C. Ginther, C. S. Chan, M. Novotny, D. J. Slamon, G. D. Plowman, A homologue of *Drosophila aurora* kinase is oncogenic and amplified in human colorectal cancers. *EMBO J.* **17**, 3052–3065 (1998).
48. P. A. Eyers, E. Erikson, L. G. Chen, J. L. Maller, A novel mechanism for activation of the protein kinase Aurora A. *Curr. Biol.* **13**, 691–697 (2003).
49. R. Bayliss, T. Sardon, I. Vernos, E. Conti, Structural basis of Aurora-A activation by TPX2 at the mitotic spindle. *Mol. Cell* **12**, 851–862 (2003).
50. P. A. Eyers, J. L. Maller, Regulation of *Xenopus* Aurora A activation by TPX2. *J. Biol. Chem.* **279**, 9008–9015 (2004).
51. S. G. Burgess, M. Mukherjee, S. Sabir, N. Joseph, C. Gutiérrez-Caballero, M. W. Richards, N. Huguenin-Dezot, J. W. Chin, E. J. Kennedy, M. Pfuhl, S. J. Royle, F. Gergely, R. Bayliss, Mitotic spindle association of TACC3 requires Aurora-A-dependent stabilization of a cryptic α -helix. *EMBO J.* **37**, e97902 (2018).
52. L. Macúrek, A. Lindqvist, D. Lim, M. A. Lampson, R. Klompaker, R. Freire, C. Clouin, S. S. Taylor, M. B. Yaffe, R. H. Medema, Polo-like kinase-1 is activated by aurora A to promote checkpoint recovery. *Nature* **455**, 119–123 (2008).
53. M. Carmena, W. C. Earnshaw, The cellular geography of aurora kinases. *Nat. Rev. Mol. Cell Biol.* **4**, 842–854 (2003).
54. N. Hégarat, E. Smith, G. Nayak, S. Takeda, P. A. Eyers, H. Hochegger, Aurora A and Aurora B jointly coordinate chromosome segregation and anaphase microtubule dynamics. *J. Cell Biol.* **195**, 1103–1113 (2011).
55. G. Bertolin, A.-L. Bulteau, M.-C. Alves-Guerra, A. Burel, M.-T. Lavault, O. Gavard, S. Le Bras, J.-P. Gagné, G. G. Poirier, R. Le Borgne, C. Prigent, M. Tramier, Aurora kinase A localises to mitochondria to control organelle dynamics and energy production. *eLife* **7**, e38111 (2018).
56. N. S. Kosower, E. M. Kosower, [1] Diamide: An oxidant probe for thiols. *Methods Enzymol.* **251**, 123–133 (1995).
57. K. M. Humphries, C. Juliano, S. S. Taylor, Regulation of cAMP-dependent protein kinase activity by glutathionylation. *J. Biol. Chem.* **277**, 43505–43511 (2002).
58. L. E. Littlepage, H. Wu, T. Andresson, J. K. Deanehan, L. T. Amundadottir, J. V. Ruderman, Identification of phosphorylated residues that affect the activity of the mitotic kinase Aurora-A. *Proc. Natl. Acad. Sci. U.S.A.* **99**, 15440–15445 (2002).
59. A. O. Walter, W. Seghezzi, W. Korver, J. Sheung, E. Lees, The mitotic serine/threonine kinase Aurora2/AIK is regulated by phosphorylation and degradation. *Oncogene* **19**, 4906–4916 (2000).
60. O. Rudyk, P. Eaton, Biochemical methods for monitoring protein thiol redox states in biological systems. *Redox Biol.* **2**, 803–813 (2014).
61. D. Sheehan, Detection of redox-based modification in two-dimensional electrophoresis proteomic separations. *Biochem. Biophys. Res. Commun.* **349**, 455–462 (2006).
62. H. S. Chung, S.-B. Wang, V. Venkatraman, C. I. Murray, J. E. Van Eyk *et al.*, *Circ. Res.* **112**, 382–392 (2013).
63. C. Maller, E. Schröder, P. Eaton, Glyceraldehyde 3-phosphate dehydrogenase is unlikely to mediate hydrogen peroxide signaling: Studies with a novel anti-dimedone sulfenic acid antibody. *Antioxid. Redox Signal.* **14**, 49–60 (2011).
64. İ. Soylu, S. M. Marino, Cy-preds: An algorithm and a web service for the analysis and prediction of cysteine reactivity. *Proteins* **84**, 278–291 (2016).
65. K. M. Humphries, M. S. Deal, S. S. Taylor, Enhanced dephosphorylation of cAMP-dependent protein kinase by oxidation and thiol modification. *J. Biol. Chem.* **280**, 2750–2758 (2005).
66. D. P. Byrne, M. Vonderach, S. Ferries, P. J. Brownridge, C. E. Eyers, P. A. Eyers, cAMP-dependent protein kinase (PKA) complexes probed by complementary differential scanning fluorimetry and ion mobility-mass spectrometry. *Biochem. J.* **473**, 3159–3175 (2016).
67. D. M. Foulkes, D. P. Byrne, W. Yeung, S. Shrestha, F. P. Bailey, S. Ferries, C. E. Eyers, K. Keeshan, C. Wells, D. H. Drewry, W. J. Zuercher, N. Kannan, P. A. Eyers, Covalent inhibitors of EGFR family protein kinases induce degradation of human Tribbles 2 (TRIB2) pseudokinase in cancer cells. *Sci. Signal.* **11**, eaat7951 (2018).
68. S. G. Burgess, R. Bayliss, The structure of C290A: C393A Aurora A provides structural insights into kinase regulation. *Acta Crystallogr. F Struct. Biol. Commun.* **71**, 315–319 (2015).
69. T. A. Kufer, H. H. W. Silljé, R. Körner, O. J. Gruss, P. Meraldi, E. A. Nigg, Human TPX2 is required for targeting Aurora-A kinase to the spindle. *J. Cell Biol.* **158**, 617–623 (2002).
70. A. Zorba, V. Buosi, S. Kutter, N. Kern, F. Pontiggia, Y.-J. Cho, D. Kern, Molecular mechanism of Aurora A kinase autophosphorylation and its allosteric activation by TPX2. *eLife* **3**, e02667 (2014).
71. C. A. Dodson, R. Bayliss, Activation of Aurora-A kinase by protein partner binding and phosphorylation are independent and synergistic. *J. Biol. Chem.* **287**, 1150–1157 (2012).
72. E. F. Ruff, J. M. Muretta, A. R. Thompson, E. W. Lake, S. Cyphers, S. K. Albanese, S. M. Hanson, J. M. Behr, D. D. Thomas, J. D. Chodera, N. M. Levinson, A dynamic mechanism for allosteric activation of Aurora kinase A by activation loop phosphorylation. *eLife* **7**, e32766 (2018).
73. K. Kinoshita, T. L. Noetzel, L. Pelletier, K. Mechtler, D. N. Drechsel, A. Schwager, M. Lee, J. W. Raff, A. A. Hyman, Aurora A phosphorylation of TACC3/maskin is required for centrosome-dependent microtubule assembly in mitosis. *J. Cell Biol.* **170**, 1047–1055 (2005).
74. R. K. Tyler, N. Shpiro, R. Marquez, P. A. Eyers, VX-680 inhibits Aurora A and Aurora B kinase activity in human cells. *Cell Cycle* **6**, 2846–2854 (2007).
75. D. N. Criddle, S. Gillies, H. K. Baumgartner-Wilson, M. Jaffar, E. C. Chinje, S. Passmore, M. Chvanov, S. Barrow, O. V. Gerasimenko, A. V. Tepikin, Menadione-induced reactive oxygen species generation via redox cycling promotes apoptosis of murine pancreatic acinar cells. *J. Biol. Chem.* **281**, 40485–40492 (2006).
76. V. Askoxylakis, G. Millonig, U. Wirkner, C. Schwager, S. Rana, A. Altmann, U. Haberkorn, J. Debus, S. Mueller, P. E. Huber, Investigation of tumor hypoxia using a two-enzyme system for in vitro generation of oxygen deficiency. *Radiat. Oncol.* **6**, 35 (2011).
77. S. Mueller, G. Millonig, G. Waite, The GOX/CAT system: A novel enzymatic method to independently control hydrogen peroxide and hypoxia in cell culture. *Adv. Med. Sci.* **54**, 121–135 (2009).
78. T. H. Truong, P. M.-U. Ung, P. B. Palde, C. E. Paulsen, A. Schlessinger, K. S. Carroll, Molecular basis for redox activation of epidermal growth factor receptor kinase. *Cell Chem. Biol.* **23**, 837–848 (2016).
79. T. J. Tavender, N. J. Bulleid, Peroxiredoxin IV protects cells from oxidative stress by removing H₂O₂ produced during disulphide formation. *J. Cell Sci.* **123**, 2672–2679 (2010).
80. J. van der Reest, S. Lilla, L. Zheng, S. Zanivan, E. Gottlieb, Proteome-wide analysis of cysteine oxidation reveals metabolic sensitivity to redox stress. *Nat. Commun.* **9**, 1581 (2018).
81. Y.-M. Go, J. D. Chandler, D. P. Jones, The cysteine proteome. *Free Radic. Biol. Med.* **84**, 227–245 (2015).
82. P. A. Eyers, K. Keeshan, N. Kannan, Tribbles in the 21st century: The evolving roles of tribbles pseudokinases in biology and disease. *Trends Cell Biol.* **27**, 284–298 (2017).
83. D. A. Smith, W. M. Toone, D. Chen, J. Bähler, N. Jones, B. A. Morgan, J. Quinn, The *Srk1* protein kinase is a target for the *Sty1* stress-activated MAPK in fission yeast. *J. Biol. Chem.* **277**, 33411–33421 (2002).
84. D. Stokoe, D. G. Campbell, S. Nakielnny, H. Hidaka, S. J. Leever, C. Marshall, P. Cohen, MAPKAP kinase-2; a novel protein kinase activated by mitogen-activated protein kinase. *EMBO J.* **11**, 3985–3994 (1992).
85. F. D. Smith, J. L. Esseltine, P. J. Nygren, D. Veessler, D. P. Byrne, M. Vonderach, I. Strashnov, C. E. Eyers, P. A. Eyers, L. K. Langeberg, J. D. Scott, Local protein kinase A action proceeds through intact holoenzymes. *Science* **356**, 1288–1293 (2017).
86. D. R. Gupta, S. K. Paul, Y. Oowatari, Y. Matsuo, M. Kawamukai, Multistep regulation of protein kinase A in its localization, phosphorylation and binding with a regulatory subunit in fission yeast. *Curr. Genet.* **57**, 353–365 (2011).
87. S. López-Avilés, M. Grande, M. González, A.-L. Helgesen, V. Alemany, M. Sanchez-Piris, O. Bachs, J. B. A. Millar, R. Aligue, Inactivation of the *Cdc25* phosphatase by the stress-activated *Srk1* kinase in fission yeast. *Mol. Cell* **17**, 49–59 (2005).
88. A. E. Leroux, J. O. Schulze, R. M. Biondi, AGC kinases, mechanisms of regulation and innovative drug development. *Semin. Cancer Biol.* **48**, 1–17 (2018).
89. G. Combes, I. Alharbi, L. G. Braga, S. Elowe, Playing polo during mitosis: PLK1 takes the lead. *Oncogene* **36**, 4819–4827 (2017).
90. P. J. Scutt, M. L. H. Chu, D. A. Sloane, M. Cherry, C. R. Bignell, D. H. Williams, P. A. Eyers, Discovery and exploitation of inhibitor-resistant aurora and polo kinase mutants for the analysis of mitotic networks. *J. Biol. Chem.* **284**, 15880–15893 (2009).
91. D. Caron, D. P. Byrne, P. Thebault, D. Soulet, C. R. Landry, P. A. Eyers, S. Elowe, Mitotic phosphotyrosine network analysis reveals that tyrosine phosphorylation regulates Polo-like kinase 1 (PLK1). *Sci. Signal.* **9**, rs14 (2016).
92. M. Bettencourt-Dias, A. Rodrigues-Martins, L. Carpenter, M. Riparbelli, L. Lehmann, M. K. Gatt, N. Carmo, F. Balloux, G. Callaini, D. Glover, SAK/PLK4 is required for centriole duplication and flagella development. *Curr. Biol.* **15**, 2199–2207 (2005).
93. R. Habadanck, Y.-D. Stierhof, C. J. Wilkinson, E. A. Nigg, The Polo kinase Plk4 functions in centriole duplication. *Nat. Cell Biol.* **7**, 1140–1146 (2005).
94. G. Manning, D. B. Whyte, R. Martinez, T. Hunter, S. Sudarsanam, The protein kinase complement of the human genome. *Science* **298**, 1912–1934 (2002).
95. Y. Wang, Y.-M. Lee, L. Baitsch, A. Huang, Y. Xiang, H. Tong, A. Lako, T. Von, C. Choi, E. Lim, J. Min, L. Li, F. Stegmeier, R. Schlegel, M. J. Eck, N. S. Gray, T. J. Mitchison, J. J. Zhao, MELK is an oncogenic kinase essential for mitotic progression in basal-like breast cancer cells. *eLife* **3**, e01763 (2014).

96. M. Beullens, S. Vancauwenbergh, N. Morrice, R. Derua, H. Ceulemans, E. Waelkens, M. Bollen *et al.*, *J. Biol. Chem.* **280**, 40003–40011 (2005).
97. X. Huang, M. Begley, K. A. Morgenstern, Y. Gu, P. Rose, H. Zhao, X. Zhu, Crystal structure of an inactive Akt2 kinase domain. *Structure* **11**, 21–30 (2003).
98. H. Xiao, M. P. Jedrychowski, D. K. Schweppe, E. L. Huttlin, Q. Yu, D. E. Heppner, J. Li, J. Long, E. L. Mills, J. Szpyt, Z. He, G. Du, R. Garrity, A. Reddy, L. P. Vaites, J. A. Paulo, T. Zhang, N. S. Gray, S. P. Gygi, E. T. Chouchani, A quantitative tissue-specific landscape of protein redox regulation during aging. *Cell* **180**, 968–983.e24 (2020).
99. J. W. Zmijewski, S. Banerjee, H. Bae, A. Friggeri, E. R. Lazarowski, E. Abraham, Exposure to hydrogen peroxide induces oxidation and activation of AMP-activated protein kinase. *J. Biol. Chem.* **285**, 33154–33164 (2010).
100. N. J. Bright, C. Thornton, D. Carling, The regulation and function of mammalian AMPK-related kinases. *Acta Physiol.* **196**, 15–26 (2009).
101. T. Kambe, T. Song, T. Takata, N. Hatano, Y. Miyamoto, N. Nozaki, Y. Naito, H. Tokumitsu, Y. Watanabe, Inactivation of Ca²⁺/calmodulin-dependent protein kinase I by S-glutathionylation of the active-site cysteine residue. *FEBS Lett.* **584**, 2478–2484 (2010).
102. J. R. Erickson, M.-I. A. Joiner, X. Guan, W. Kutschke, J. Yang, C. V. Oddis, R. K. Bartlett, J. S. Lowe, S. E. O'Donnell, N. Aykin-Burns, M. C. Zimmerman, K. Zimmerman, A.-J. L. Ham, R. M. Weiss, D. R. Spitz, M. A. Shea, R. J. Colbran, P. J. Mohler, M. E. Anderson, A dynamic pathway for calcium-independent activation of CaMKII by methionine oxidation. *Cell* **133**, 462–474 (2008).
103. A. K. Leonberg, Y.-C. Chai, The functional role of cysteine residues for c-Abl kinase activity. *Mol. Cell. Biochem.* **304**, 207–212 (2007).
104. Y. Tsuchiya, D. P. Byrne, S. G. Burgess, J. Bormann, J. Baković, Y. Huang, A. Zhyvoloup, B. Y. K. Yu, S. Peak-Chew, T. Tran, F. Bellamy, A. B. Tabor, A. E. Chan, L. Guruprasad, O. Garifulin, V. Filonenko, M. Vonderach, S. Ferries, C. E. Eyers, J. Carroll, M. Skehel, R. Bayliss, P. A. Eyers, I. Gout, Covalent Aurora A regulation by the metabolic integrator coenzyme A. *Redox Biol.* **28**, 101318 (2020).
105. J. Beenstock, N. Mooshayef, D. Engelberg, How do protein kinases take a selfie (autophosphorylate)? *Trends Biochem. Sci.* **41**, 938–953 (2016).
106. L. R. Pearce, D. Komander, D. R. Alessi, The nuts and bolts of AGC protein kinases. *Nat. Rev. Mol. Cell Biol.* **11**, 9–22 (2010).
107. H. Murata, Y. Ihara, H. Nakamura, J. Yodoi, K. Sumikawa, T. Kondo, Glutaredoxin exerts an anti-apoptotic effect by regulating the redox state of Akt. *J. Biol. Chem.* **278**, 50226–50233 (2003).
108. W. C. Burhans, N. H. Heintz, The cell cycle is a redox cycle: Linking phase-specific targets to cell fate. *Free Radic. Biol. Med.* **47**, 1282–1293 (2009).
109. J. Chiu, I. W. Dawes, Redox control of cell proliferation. *Trends Cell Biol.* **22**, 592–601 (2012).
110. G.-F. Wang, Q. Dong, Y. Bai, J. Yuan, Q. Xu, C. Cao, X. Liu, Oxidative stress induces mitotic arrest by inhibiting Aurora A-involved mitotic spindle formation. *Free Radic. Biol. Med.* **103**, 177–187 (2017).
111. N. Brandes, S. Schmitt, U. Jakob, Thiol-based redox switches in eukaryotic proteins. *Antioxid. Redox Signal.* **11**, 997–1014 (2009).
112. T. H. Truong, K. S. Carroll, Redox regulation of protein kinases. *Crit. Rev. Biochem. Mol. Biol.* **48**, 332–356 (2013).
113. M. Saitoh, H. Nishitoh, M. Fujii, K. Takeda, K. Tobiume, Y. Sawada, M. Kawabata, K. Miyazono, H. Ichijo, Mammalian thioredoxin is a direct inhibitor of apoptosis signal-regulating kinase (ASK). *EMBO J.* **17**, 2596–2606 (1998).
114. H.-S. Park, J.-W. Yu, J.-H. Cho, M.-S. Kim, S.-H. Huh, K. Ryoo, E.-J. Choi, Inhibition of apoptosis signal-regulating kinase 1 by nitric oxide through a thiol redox mechanism. *J. Biol. Chem.* **279**, 7584–7590 (2004).
115. Y. Diao, W. Liu, C. C. L. Wong, X. Wang, K. Lee, P.-y. Cheung, L. Pan, T. Xu, J. Han, J. R. Yates III, M. Zhang, Z. Wu, Oxidation-induced intramolecular disulfide bond inactivates mitogen-activated protein kinase kinase 6 by inhibiting ATP binding. *Proc. Natl. Acad. Sci. U.S.A.* **107**, 20974–20979 (2010).
116. D. Wilhelm, K. Bender, A. Knebel, P. Angel, The level of intracellular glutathione is a key regulator for the induction of stress-activated signal transduction pathways including Jun N-terminal protein kinases and p38 kinase by alkylating agents. *Mol. Cell. Biol.* **17**, 4792–4800 (1997).
117. R. M. Jarvis, S. M. Hughes, E. C. Ledgerwood, Peroxiredoxin 1 functions as a signal peroxidase to receive, transduce, and transmit peroxide signals in mammalian cells. *Free Radic. Biol. Med.* **53**, 1522–1530 (2012).
118. S. Stöcker, M. Maurer, T. Ruppert, T. P. Dick, A role for 2-Cys peroxiredoxins in facilitating cytosolic protein thiol oxidation. *Nat. Chem. Biol.* **14**, 148–155 (2018).
119. D. Peralta, A. K. Bronowska, B. Morgan, E. Dóka, K. Van Laer, P. Nagy, F. Gräter, T. P. Dick, A proton relay enhances H₂O₂ sensitivity of GAPDH to facilitate metabolic adaptation. *Nat. Chem. Biol.* **11**, 156–163 (2015).
120. L. B. Poole, The basics of thiols and cysteines in redox biology and chemistry. *Free Radic. Biol. Med.* **80**, 148–157 (2015).
121. M. S. Bharadwaj, D. J. Tyrrell, I. Leng, J. L. Demons, M. F. Lyles, J. J. Carr, B. J. Nicklas, A. J. A. Molina, Relationships between mitochondrial content and bioenergetics with obesity, body composition and fat distribution in healthy older adults. *BMC Obes.* **2**, 40 (2015).
122. D. C. Wallace, Mitochondria and cancer. *Nat. Rev. Cancer* **12**, 685–698 (2012).
123. S. Arun, L. Liu, G. Donmez, Mitochondrial biology and neurological diseases. *Curr. Neuropharmacol.* **14**, 143–154 (2016).
124. J. G. Gill, E. Piskounova, S. J. Morrison, Cancer, oxidative stress, and metastasis. *Cold Spring Harb. Symp. Quant. Biol.* **81**, 163–175 (2016).
125. E. W. Lake, J. M. Muretta, A. R. Thompson, D. M. Rasmussen, A. Majumdar, E. B. Faber, E. F. Ruff, D. D. Thomas, N. M. Levinson, Quantitative conformational profiling of kinase inhibitors reveals origins of selectivity for Aurora kinase activation states. *Proc. Natl. Acad. Sci. U.S.A.* **115**, E11894–E11903 (2018).
126. W. Pitsawong, V. Buosi, R. Otten, R. V. Agafonov, A. Zorba, N. Kern, S. Kutter, G. Kern, R. A. P. Pádua, X. Meniche, D. Kern, Dynamics of human protein kinase Aurora A linked to drug selectivity. *eLife* **7**, e36656 (2018).
127. M. Singh, H. R. Jadhav, Targeting non-small cell lung cancer with small-molecule EGFR tyrosine kinase inhibitors. *Drug Discov. Today* **23**, 745–753 (2018).
128. J. Bain, L. Plater, M. Elliott, N. Shpiro, C. J. Hastie, H. McLauchlan, I. Klevernic, J. S. C. Arthur, D. R. Alessi, P. Cohen, The selectivity of protein kinase inhibitors: A further update. *Biochem. J.* **408**, 297–315 (2007).
129. D. I. McSkimming, S. Dastgheib, T. R. Baffi, D. P. Byrne, S. Ferries, S. T. Scott, A. C. Newton, C. E. Eyers, K. J. Kochut, P. A. Eyers, N. Kannan, KinView: A visual comparative sequence analysis tool for integrated kinome research. *Mol. Biosyst.* **12**, 3651–3665 (2016).
130. S. Mohanty, K. Oruganty, A. Kwon, D. P. Byrne, S. Ferries, Z. Ruan, L. E. Hanold, S. Katiyar, E. J. Kennedy, P. A. Eyers, N. Kannan, Hydrophobic core variations provide a structural framework for tyrosine kinase evolution and functional specialization. *PLoS Genet.* **12**, e1005885 (2016).
131. D. P. Byrne, Y. Li, P. Ngamlert, K. Ramakrishnan, C. E. Eyers, C. Wells, D. H. Drewry, W. J. Zuercher, N. G. Berry, D. G. Fernig, P. A. Eyers, New tools for evaluating protein tyrosine sulfation: Tyrosylprotein sulfotransferases (TPSTs) are novel targets for RAF protein kinase inhibitors. *Biochem. J.* **475**, 2435–2455 (2018).
132. J. M. Murphy, Q. Zhang, S. N. Young, M. L. Reese, F. P. Bailey, P. A. Eyers, D. Ungureanu, H. Hammaren, O. Silvennoinen, L. N. Varghese, K. Chen, A. Tripaydonis, N. Jura, K. Fukuda, J. Qin, Z. Nimchuk, M. B. Mudgett, S. Elowe, C. L. Gee, L. Liu, R. J. Daly, G. Manning, J. J. Babon, I. S. Lucet, A robust methodology to subclassify pseudokinases based on their nucleotide-binding properties. *Biochem. J.* **457**, 323–334 (2014).
133. S. Lu, Y. Cao, S.-B. Fan, Z.-L. Chen, R.-Q. Fang, S.-M. He, M.-Q. Dong, Mapping disulfide bonds from sub-micrograms of purified proteins or micrograms of complex protein mixtures. *Biophys. Rep.* **4**, 68–81 (2018).
134. M. Mormann, J. Eble, C. Schwöppe, R. M. Mesters, W. E. Berdel, J. Peter-Katalinic, G. Pohlentz, Fragmentation of intra-peptide and inter-peptide disulfide bonds of proteolytic peptides by nanoESI collision-induced dissociation. *Anal. Bioanal. Chem.* **392**, 831–838 (2008).
135. A. F. Neuwald, Rapid detection, classification and accurate alignment of up to a million or more related protein sequences. *Bioinformatics* **25**, 1869–1875 (2009).
136. N. Kannan, S. S. Taylor, Y. Zhai, J. C. Venter, G. Manning, Structural and functional diversity of the microbial kinome. *PLoS Biol.* **5**, e17 (2007).
137. R. D. Finn, J. Mistry, J. Tate, P. Coghill, A. Heger, J. E. Pollington, O. L. Gavin, P. Gunasekaran, G. Ceric, K. Forslund, L. Holm, E. L. L. Sonnhammer, S. R. Eddy, A. Bateman, The Pfam protein families database. *Nucleic Acids Res.* **38**, D211–D222 (2010).
138. E. Talevich, A. Mirza, N. Kannan, Structural and evolutionary divergence of eukaryotic protein kinases in Apicomplexa. *BMC Evol. Biol.* **11**, 321 (2011).
139. UniProt Consortium, UniProt: A hub for protein information. *Nucleic Acids Res.* **43**, D204–D212 (2015).
140. E. W. Sayers, T. Barrett, D. A. Benson, S. H. Bryant, K. Canese, V. Chetvernin, D. M. Church, M. DiCuccio, R. Edgar, S. Federhen, M. Feolo, L. Y. Geer, W. Helmsberg, Y. Kapustin, D. Landsman, D. J. Lipman, T. L. Madden, D. R. Maglott, V. Miller, I. Mizrahi, J. Ostell, K. D. Pruitt, G. D. Schuler, E. Sequeira, S. T. Sherry, M. Shumway, K. Sirotkin, A. Souvorov, G. Starchenko, T. A. Tatusova, L. Wagner, E. Yaschenko, J. Ye, Database resources of the National Center for Biotechnology Information. *Nucleic Acids Res.* **37**, D5–D15 (2009).
141. T. D. Schneider, R. M. Stephens, Sequence logos: A new way to display consensus sequences. *Nucleic Acids Res.* **18**, 6097–6100 (1990).
142. S. Moreno, A. Klar, P. Nurse, Molecular genetic analysis of fission yeast *Schizosaccharomyces pombe*. *Methods Enzymol.* **194**, 795–823 (1991).
143. R. A. Craven, D. J. Griffiths, K. S. Sheldrick, R. E. Randall, I. M. Hagan, A. M. Carr, Vectors for the expression of tagged proteins in *Schizosaccharomyces pombe*. *Gene* **221**, 59–68 (1998).

144. A. Delaunay, A. D. Isnard, M. B. Toledano, H₂O₂ sensing through oxidation of the Yap1 transcription factor. *EMBO J.* **19**, 5157–5166 (2000).
145. A. M. Day, E. A. Veal, Hydrogen peroxide-sensitive cysteines in the Sty1 MAPK regulate the transcriptional response to oxidative stress. *J. Biol. Chem.* **285**, 7505–7516 (2010).
146. B. A. Wolfe, K. L. Gould, Fission yeast Clp1p phosphatase affects G2/M transition and mitotic exit through Cdc25p inactivation. *EMBO J.* **23**, 919–929 (2004).
147. T. Higuchi, Y. Watanabe, M. Yamamoto, Protein kinase A regulates sexual development and gluconeogenesis through phosphorylation of the Zn finger transcriptional activator Rst2p in fission yeast. *Mol. Cell. Biol.* **22**, 1–11 (2002).

Acknowledgments: We thank K. Gould and M. Yamamoto for *S. pombe* strains and J. Hastie and H. McLauchlan for assistance with protein kinase reagents. We also thank S. Evans for media preparation and outstanding technical support. **Funding:** This work was funded by a Royal Society Research Grant (to P.A.E.), BBSRC TRDF grant B/N021703/1 (to P.A.E.), a BBSRC DTP studentship (BB/M011186/1 to M.G. and E.A.V.), BBSRC project grant BB/T002484/1 (to E.A.V.), and North West Cancer Research grants CR1097 and CR1208 (to D.P.B. and P.A.E.). Funding for N.K. from the NIH (R01GM114409) is also acknowledged. **Author contributions:**

P.A.E., N.K., C.E.E., and E.A.V. obtained the funding and designed the experiments collaboratively alongside D.P.B., M.G., M.C., A.E.C., and L.A.D., who performed the experiments. S.S. and N.K. performed the bioinformatics analysis, and D.P.B. and P.A.E. wrote the paper, with contributions from all authors, who also approved the final version before submission.

Competing interests: The authors declare that they have no competing interests. **Data and materials availability:** All data needed to evaluate conclusions made are available in the main text or the Supplementary Materials of the paper.

Submitted 8 March 2019
Resubmitted 6 February 2020
Accepted 7 May 2020
Published 7 July 2020
10.1126/scisignal.aax2713

Citation: D. P. Byrne, S. Shrestha, M. Galler, M. Cao, L. A. Daly, A. E. Campbell, C. E. Eyers, E. A. Veal, N. Kannan, P. A. Eyers, Aurora A regulation by reversible cysteine oxidation reveals evolutionarily conserved redox control of Ser/Thr protein kinase activity. *Sci. Signal.* **13**, eaax2713 (2020).

Aurora A regulation by reversible cysteine oxidation reveals evolutionarily conserved redox control of Ser/Thr protein kinase activity

Dominic P. Byrne, Safal Shrestha, Martin Galler, Min Cao, Leonard A. Daly, Amy E. Campbell, Claire E. Eyers, Elizabeth A. Veal, Natarajan Kannan and Patrick A. Eyers

Sci. Signal. **13** (639), eaax2713.
DOI: 10.1126/scisignal.aax2713

Kinase regulation conserved under stress

Oxidative stress is necessary for normal cellular function and tissue physiology but can also be pathological, and its effects are mediated in part through functional modification of various proteins. Shrestha *et al.* and Byrne *et al.* found that the oxidation of kinases at active site-adjacent cysteine residues, which were conserved across the eukaryotic kinome, regulated cell metabolism and mitosis. Shrestha *et al.* found that conserved cysteine residues within the diabetes-associated metabolic kinase FN3K acted as a toggle switch upon oxidation, promoting its functional oligomerization and consequently altering cellular redox status. Byrne *et al.* found that oxidation of mitotic kinases in human cells and yeast suppressed kinase catalytic activity and, in yeast, impaired cellular division. Exploring the effect of chronic oxidative stress on kinase function and how that may be spatiotemporally regulated may enable the development of new targeted therapeutics.

ARTICLE TOOLS

<http://stke.sciencemag.org/content/13/639/eaax2713>

SUPPLEMENTARY MATERIALS

<http://stke.sciencemag.org/content/suppl/2020/07/02/13.639.eaax2713.DC1>

RELATED CONTENT

<http://stke.sciencemag.org/content/sigtrans/13/615/eaay7315.full>
<http://stke.sciencemag.org/content/sigtrans/13/641/eabd8558.full>
<http://stke.sciencemag.org/content/sigtrans/13/641/eabb6707.full>

REFERENCES

This article cites 146 articles, 51 of which you can access for free
<http://stke.sciencemag.org/content/13/639/eaax2713#BIBL>

PERMISSIONS

<http://www.sciencemag.org/help/reprints-and-permissions>

Use of this article is subject to the [Terms of Service](#)

Science Signaling (ISSN 1937-9145) is published by the American Association for the Advancement of Science, 1200 New York Avenue NW, Washington, DC 20005. The title *Science Signaling* is a registered trademark of AAAS.

Copyright © 2020 The Authors, some rights reserved; exclusive licensee American Association for the Advancement of Science. No claim to original U.S. Government Works